REVIEW ARTICLE

Femtosecond pulse shaping using spatial light modulators

A. M. Weiner[a)]
School of Electrical and Computer Engineering, Purdue University, West Lafayette, Indiana 47907-1285

(Received 17 August 1999; accepted for publication 20 January 2000)

We review the field of femtosecond pulse shaping, in which Fourier synthesis methods are used to generate nearly arbitrarily shaped ultrafast optical wave forms according to user specification. An emphasis is placed on programmable pulse shaping methods based on the use of spatial light modulators. After outlining the fundamental principles of pulse shaping, we then present a detailed discussion of pulse shaping using several different types of spatial light modulators. Finally, new research directions in pulse shaping, and applications of pulse shaping to optical communications, biomedical optical imaging, high power laser amplifiers, quantum control, and laser-electron beam interactions are reviewed. © *2000 American Institute of Physics.* [S0034-6748(00)02005-0]

I. INTRODUCTION

Since the advent of the laser nearly 40 years ago, there has been a sustained interest in the quest to generate ultrashort laser pulses in the picosecond (10^{-12} s) and femtosecond (10^{-15} s) range. Reliable generation of pulses below 100 fs in duration occurred for the first time in 1981 with the invention of the colliding pulse modelocked (CPM) ring dye laser.[1] Subsequent nonlinear pulse compression of pulses from the CPM laser led to a series of even shorter pulses,[2–6] culminating in pulses as short as 6 fs, a record which stood for over a decade. Six femtoseconds in the visible corresponds to only three optical cycles, and therefore such pulse durations are approaching the fundamental single optical cycle limit. Further rapid progress occurred following the demonstration of femtosecond pulse generation from solid-state laser media in the 1990 time frame.[7] Femtosecond solid-state lasers bring a number of important advantages compared to their liquid dye laser counterparts, including substantially improved output power and stability and new physical mechanisms for pulse generation advantageous for production of extremely short pulses. Femtosecond solid-state laser technology has now advanced to the point that pulses below 6 fs can be generated directly from the laser.[8–14] Equally important, the use of solid-state gain media has also led to simple, turn-key femtosecond lasers, and many researchers are now setting their sights on practical and low cost ultrafast laser systems suitable for real-world applications (in addition to the scientific applications for which femtosecond lasers have been used extensively). Detailed information on the current status of femtosecond technology and applications can be found in several recent journal special issues,[15–17] books,[18–21] and in another recent review article in this journal.[22]

The focus of this article is femtosecond pulse shaping, a topic complementary to femtosecond pulse generation. Over the past decade powerful optical waveform synthesis (or pulse shaping) methods have been developed which allow generation of complicated ultrafast optical waveforms according to user specification. Pulse shaping systems have already demonstrated a strong impact as an experimental tool providing unprecedented control over ultrafast laser waveforms for ultrafast spectroscopy, nonlinear fiber optics, and high-field physics. Coupled with the recent advances and resulting widespread availability of femtosecond lasers, as well as advances in femtosecond pulse characterization techniques, femtosecond pulse shaping is poised to impact many diverse and additional applications. In the terminology of electronic instrumentation, femtosecond lasers constitute the world's best pulse generators, while pulse shaping is the short pulse optical analog to electronic function generators, which widely provide electronic square waves, triangle waves, and indeed arbitrary user specified waveforms.

A number of approaches for ultrafast pulse shaping have been advanced. Here we concentrate on the most successful and widely adopted method, in which waveform synthesis is achieved by spatial masking of the spatially dispersed optical frequency spectrum. A key point is that because waveform synthesis is achieved by parallel modulation in the frequency domain, waveforms with effective serial modulation bandwidths as high as terahertz and above can be generated without requiring any ultrafast modulators. We will be particularly interested in pulse shaping using spatial light modulators (SLMs), where the SLM allows reprogrammable waveform generation under computer control. A review article by Froehly describes a variety of pulse shaping techniques investigated prior to 1983 for picosecond pulses.[23] A more recent review by Weiner provides a broad account of femtosecond pulse shaping as well as related pulse processing techniques, including both the pulse shaping technique which is the focus of the current article as well as other approaches.[27] Other useful reviews include Ref. 24, which

[a)]Electronic mail: amw@ecn.purdue.edu

describes early results on femtosecond pulse shaping using fixed masks and related experiments on picosecond pulse shaping performed in the context of nonlinear pulse compression, and Refs. 25 and 26, which include citations to recent results on pulse shaping as well as holographic and nonlinear pulse processing.

This review article is organized as follows. In Sec. II we discuss the basics of femtosecond pulse shaping, including a description of the apparatus, examples of pulse shaping results using fixed spatial masks, important results from the theory of pulse shaping, and instrument control, alignment, and pulse measurement issues. In Secs. III and IV we discuss programmable pulse shaping using liquid crystal SLMs and acoustic-optic modulators, respectively; these are the two types of SLMS which are most widely applied for femtosecond pulse shaping. Section V summarizes the relative advantages and disadvantages of liquid crystal and acousto-optic SLMs for pulse shaping. Section VI covers developments in deformable, movable, and micromechanical mirrors for pulse shaping applications. These special mirror based approaches for programmable pulse shaping, while important, are not yet as completely developed as the liquid crystal or acousto-optic approaches, and for this reason are not included for comparison in Sec. V. In Sec. VII we discuss further directions in femtosecond pulse shaping, including shaping of incoherent light, integration, direct space-to-time pulse shaping, and generalized pulse shapers for holographic and nonlinear pulse processing. We conclude in Sec. VIII by surveying some of the applications of femtosecond pulse shaping, including optical communications, dispersion compensation, laser control of terahertz radiation, coherent control of quantum mechanical processes, and laser-electron beam interaction physics.

II. FEMTOSECOND PULSE SHAPING BASICS

A. Linear filtering

The femtosecond pulse shaping approach described in this article is based on the linear, time-invariant filter, a concept well known in electrical engineering. Linear filtering is commonly used to process electrical signals ranging from low frequencies (audio and below) to very high frequencies (microwave). Here we apply to linear filtering to generate specially shaped optical waveforms on the picosecond and femtosecond time scale. Of course, the hardware needed for programmable linear filtering of femtosecond laser pulses looks very different from the familiar resistors, capacitors, and inductors used for linear filtering of conventional electrical signals.

Linear filtering can be described in either the time domain or the frequency domain, as depicted in Fig. 1.[27] In the time domain, the filter is characterized by an impulse response function $h(t)$. The output of the filter $e_{\text{out}}(t)$ in response to an input pulse $e_{\text{in}}(t)$ is given by the convolution of $e_{\text{in}}(t)$ and $h(t)$

$$e_{\text{out}}(t) = e_{\text{in}}(t) * h(t) = \int dt' e_{\text{in}}(t') h(t-t'), \tag{2.1}$$

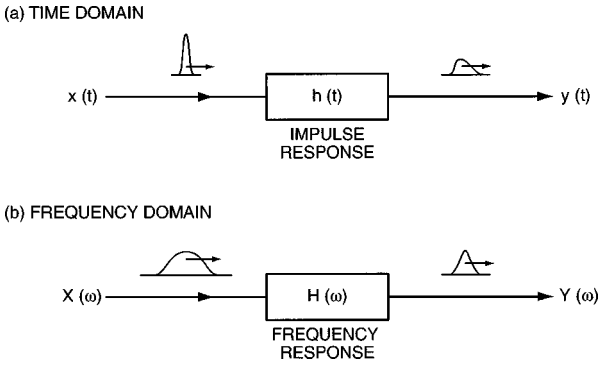

FIG. 1. Pulse shaping by linear filtering. (a) Time-domain view. (b) Frequency domain view.

where $*$ denotes convolution. If the input is a delta function, the output is simply $h(t)$. Therefore, for a sufficiently short input pulse, the problem of generating a specific output pulse shape is equivalent to the task of fabricating a linear filter with the desired impulse response. Note that instead of the term ''impulse response function,'' which is common in electrical engineering, $h(t)$ may also be called a Green function, which is a common terminology in some other fields.

In the frequency domain, the filter is characterized by its frequency response $H(\omega)$. The output of the linear filter $E_{\text{out}}(\omega)$ is the product of the input signal $E_{\text{in}}(\omega)$ and the frequency response $H(\omega)$—i.e.,

$$E_{\text{out}}(\omega) = E_{\text{in}}(\omega) H(\omega). \tag{2.2}$$

Here $e_{\text{in}}(t)$, $e_{\text{out}}(t)$, and $h(t)$ and $E_{\text{in}}(\omega)$, $E_{\text{out}}(\omega)$, and $H(\omega)$, respectively, are Fourier transform pairs—i.e.,

$$H(\omega) = \int dt\, h(t) e^{-i\omega t} \tag{2.3}$$

and

$$h(t) = \frac{1}{2\pi} \int d\omega\, H(\omega) e^{i\omega t}. \tag{2.4}$$

For a delta function input pulse, the input spectrum $E_{\text{in}}(\omega)$ is equal to unity, and the output spectrum is equal to the frequency response of the filter. Therefore, due to the Fourier transform relations, generation of a desired output waveform can be accomplished by implementing a filter with the required frequency response. Our pulse shaping approach is described most naturally by means of this frequency domain point of view.

B. Pulse shaping apparatus and pulse shaping examples using fixed masks

Figure 2 shows the basic pulse shaping apparatus, which consists of a pair of diffraction gratings and lenses, arranged in a configuration known as a ''zero dispersion pulse compressor,'' and a pulse shaping mask.[28] The individual frequency components contained within the incident (usually but not always bandwidth limited) ultrashort pulse are angularly dispersed by the first diffraction grating, and then focused to small diffraction limited spots at the back focal plane of the first lens, where the frequency components are

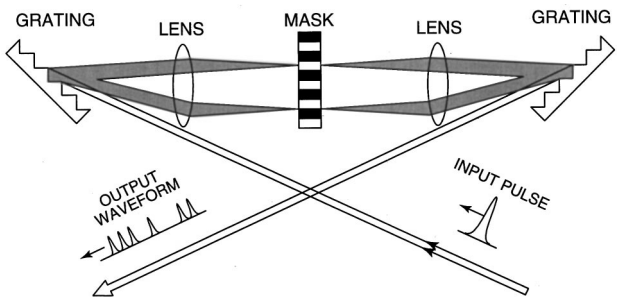

FIG. 2. Basic layout for Fourier transform femtosecond pulse shaping.

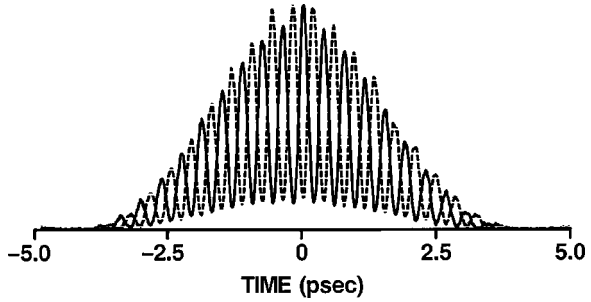

FIG. 3. Intensity cross-correlation traces of optical tone bursts resulting from a pair of isolated optical frequency components. Solid: optical frequencies in phase. Dotted: optical frequencies phase shifted by π.

spatially separated along one dimension. Essentially the first lens performs a Fourier transform which coverts the angular dispersion from the grating to a spatial separation at the back focal plane. Spatially patterned amplitude and phase masks (or a SLM) are placed in this plane in order to manipulate the spatially dispersed optical Fourier components. After a second lens and grating recombine all the frequencies into a single collimated beam, a shaped output pulse is obtained, with the output pulse shape given by the Fourier transform of the patterned transferred by the masks onto the spectrum.

In order for this technique to work as desired, one requires that in the absence of a pulse shaping mask, the output pulse should be identical to the input pulse. Therefore, the grating and lens configuration must be truly free of dispersion. This can be guaranteed if the lenses are set up as a unit magnification telescope, with the gratings located at the outside focal planes of the telescope. In this case the first lens performs a spatial Fourier transform between the plane of the first grating and the masking plane, and the second lens performs a second Fourier transform from the masking plane to the plane of the second grating. The total effect of these two consecutive Fourier transforms is that the input pulse is unchanged in traveling through the system if no pulse shaping mask is present.

Note that this dispersion-free condition also depends on several approximations, e.g., that the lenses are thin and free of aberrations, that chromatic dispersion in passing through the lenses or other elements which may be inserted into the pulse shaper is small, and that the gratings have a flat spectral response. Distortion-free propagation through the ''zero dispersion compressor'' has been observed in many experiments with pulses down to roughly 50 fs—see for example Refs. 28 and 29. For much shorter pulses, especially in the 10–20 fs range, more care must be taken to satisfy these approximations. For example, both the chromatic aberration of the lenses in the pulse shaper and the dispersion experienced in passing through the lenses can become important effects. However, by using spherical mirrors instead of lenses, these problems can be avoided and dispersion-free operation has been obtained.[30]

The first use of the pulse shaping apparatus shown in Fig. 2 was reported by Froehly, who performed pulse shaping experiments with input pulses 30 ps in duration.[23] Related experiments demonstrating shaping of pulses a few picoseconds in duration by spatial masking within a fiber and grating pulse compressor were performed independently by Heritage and Weiner;[31–33] in those experiments the grating pair was used in a dispersive configuration without internal lenses since grating dispersion was needed in order to compress the input pulses which were chirped through nonlinear propagation in the fiber. The dispersion-free apparatus in Fig. 2 was subsequently adopted by Weiner *et al.* for manipulation of pulses on the 100 fs time scale, initially using fixed pulse shaping masks[28] and later using programmable SLMs.[34,35] With minor modifications, namely, replacing the pulse shaping lenses with spherical mirrors, pulse-shaping operation has been successfully demonstrated for input pulses on the 10–20 fs time scale.[30,36–38] A fiber-pigtailed pulse shaper, with fiber-to-fiber insertion loss as low as 5.3 dB, has also been reported for 1.55 μm operation for optical communications applications.[39–41] The apparatus of Fig. 2 (without the mask) can also be used to introduce dispersion for pulse stretching or compression by changing the grating-lens spacing. This idea was introduced and analyzed by Martinez[42] and is now extensively used for high-power femtosecond chirped pulse amplifiers.[22,43]

Pulse shaping using programmable SLMs will be discussed beginning in Sec. III. Here we present several examples using fixed spatial masks, the masking technology employed in early femtosecond pulse shaping experiments. Fixed masks can provide excellent pulse shaping quality and have been employed in experimental applications of pulse shaping in nonlinear fiber optics, fiber communications, and ultrafast spectroscopy. Disadvantages of fixed masks are that they do not easily provide continuous phase variations (binary phase variations are fine) and that a new mask must be fabricated for each experiment.

Figure 3[28] shows intensity cross-correlation traces of waveforms generated by using an opaque mask with two isolated slits, resulting in a pair of distinct and isolated spectral peaks. Note that the intensity cross-correlation traces approximately provide a measurement of optical intensity versus time—see Sec. II G for further explanation. The two frequencies interfere in the time domain, producing a high-frequency optical tone burst. The 2.6 THz period of the intensity modulation is identical to the separation of the selected frequency components and corresponds to a period of only 380 fs. We have also performed experiments using an additional phase mask to impose a π phase shift between the two spectral components. The resulting waveform is shown in Fig. 3 as the dotted line. The two distinct frequencies still interfere to produce a tone burst. However, the π phase shift

is expected to lead to an interchange in the positions of the peaks and nulls of the time domain, and this effect is clearly seen in the data. It is worth noting that this effect, namely the shift in the time-domain interference features reflecting spectral phase variations, demonstrated here in the context of pulse shaping, has also been developed into a powerful pulse characterization tool for measuring the spectral phase profiles of unknown ultrashort pulses.[44] It is also worth noting that the data in Fig. 3 represent a time-domain analog of the well known Young's double slit interference experiment. This is one manifestation of the close analogy which exists between time-domain Fourier optics discussed here and the well known and active field of spatial domain Fourier optics.

We also consider generation of ultrafast square pulses using fixed masks.[28] The spectrum of a square pulse of duration T is shaped as a sinc function, given by

$$E(f)=E_0 T\frac{\sin(\pi fT)}{\pi fT}. \tag{2.5}$$

The corresponding mask is specified by

$$M(x)=\frac{\sin(\pi x/x_0)}{\pi x/x_0}, \tag{2.6}$$

where $M(x)$ is the masking function, $x_0=(T\partial f/\partial x)^{-1}$, and $\partial f/\partial x$ is the spatial dispersion at the masking plane. In order to implement the desired filtering function, both a phase and an amplitude mask are needed. The phase mask is used to impart the required alternating sign to the filter. The transmission function of the amplitude mask varies continuously with position. Furthermore, due to the combination of fast and slow temporal features (<100 fs rise and fall times, pulse duration in the picosecond range), the amplitude mask must be capable of producing a series of sidelobes over a large dynamic range. The required phase and amplitude masks were fabricated on fused silica substrates using microlithographic patterning techniques, and the two masks were placed back to back at the masking plane of the pulse shaper. Phase masks were fabricated by using reactive ion etching to produce a relief pattern on the surface of the fused silica. Amplitude masks consisted of a series of fine opaque metal lines deposited onto the substrate with linewidths and spacings varied in order to obtain the desired transmission. This approach to forming a variable transmission amplitude mask is related to diffractive optics structures utilized for spatial manipulation of laser beams via computer generated holography. Figure 4 shows a semilog plot of a power spectrum produced in this way. The data correspond to a mask containing 15 sidelobes on either side of the central peak. A dynamic range approaching 10^4:1, as well as excellent signal-to-noise ratio, are evident from the power spectrum. The dotted line, which is an actual sinc function, is in good agreement with the data, although the zeroes in the data are washed out due to the finite spectral resolution of the measurement device Figure 5(a) shows an intensity cross-correlation measurement of a 2 ps square pulse produced by using masks truncated after five sidelobes on either side of the main spectral peak. The rise and fall times of the square pulse are found to be on the order of 100 fs. The ripple

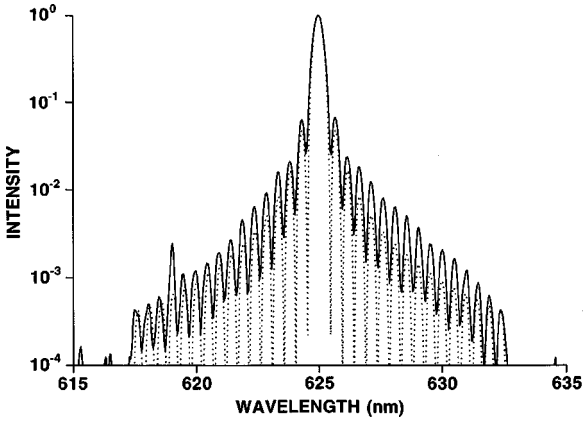

FIG. 4. Semilog plot of power spectrum of an optical square pulse.

present on the square pulse arises because of the truncation of the spectrum and is in good qualitative agreement with the theoretical intensity profile [Fig. 5(b)]. Square pulses with reduced ripple have also been obtained, by avoiding truncation of the spectrum and instead using a more gentle spectral apodization. An experimental example of such a ''smooth'' square pulse is plotted in Fig. 5(c).[45]

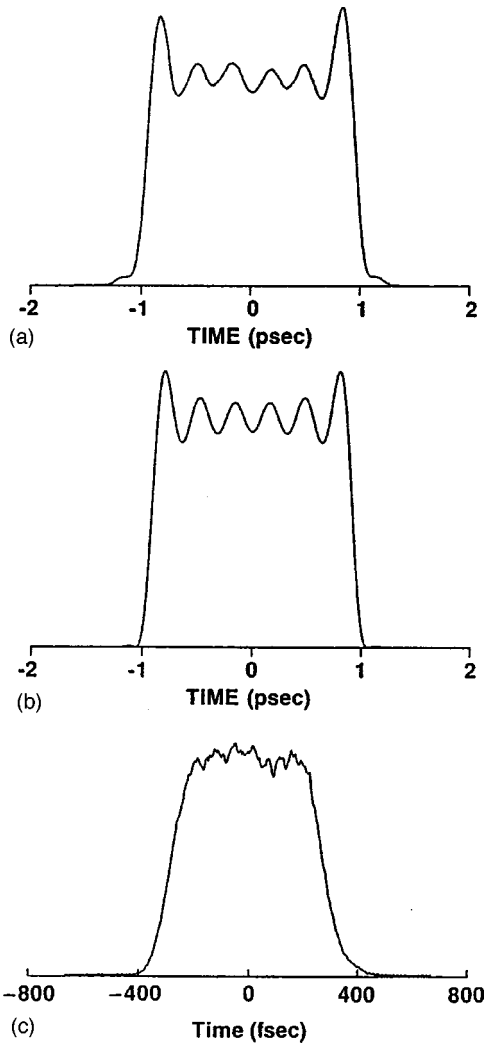

FIG. 5. Optical square pulses. (a) Measurement of a 2 ps optical square pulse. (b) Corresponding theoretical intensity profile. (c) Measurement of a square pulse with reduced ripple.

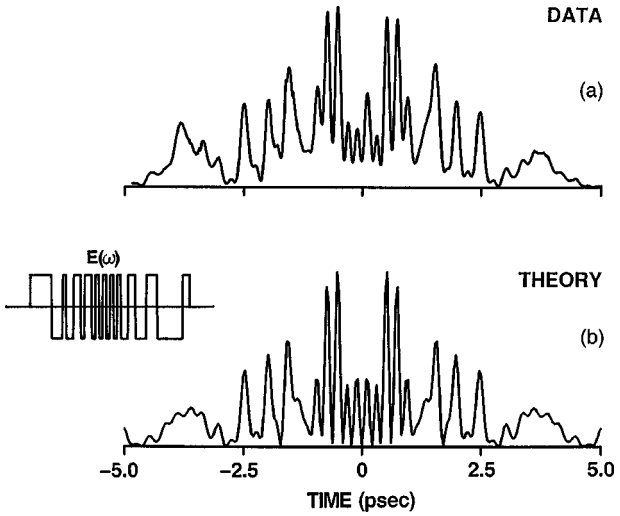

FIG. 6. Ultrafast pseudonoise bursts generated by using a pseudorandom spectral phase filter (shown as inset). (a) Intensity cross-correlation trace. (b) Corresponding theoretical intensity profile.

At this point we also discuss pulse shaping using phase-only filters. Phase-only filters have the advantage, in situations where they are adequate, of no inherent loss. Here we discuss two examples of useful pulse shaping via lossless, phase-only filtering using fixed phase masks. There are also many examples of phase-only filtering using SLMs; these will be discussed later.

One interesting example is encoding of femtosecond pulses by utilizing pseudorandom phase patterns to scramble (encode) the spectral phases.[28,29] An example is shown in Fig. 6.[29] The clear aperture of the mask is divided into 44 equal pixels, each of which corresponds to a phase shift of either zero or π. Figure 6(a) shows a measurement of the intensity profile of the encoded waveform. Spectral encoding spreads the incident femtosecond pulses into a complicated pseudonoise burst within an ~8 ps temporal envelope. The peak intensity is reduced to ~8% compared to that of an uncoded pulse of the same optical bandwidth. For comparison, the theoretical intensity profile, which is the square of the Fourier transform of the spectral phase mask, is shown in Fig. 6(b). The agreement between theory and experiment is excellent. Similar coding and decoding has been demonstrated with longer phase codes (up to 127 pixels)[28] and also using programmable SLMs.[41] An important feature is that because the phase-only filtering is lossless, by using a second pulse shaper with a conjugate phase mask, the spectral phase modulation can be undone, with the result that the pseudonoise burst is decoded (restored) back to the original ultrashort pulse duration. This forms the basis of a proposed ultrashort pulse code-division multiple-access (CDMA) communications concept, in which multiple users share a common fiber optic channel on the basis of different minimally interfering code sequences assigned to different transmitter-receiver pairs.[41,46]

In some cases only the temporal intensity profile of an output pulse is of interest, and this greatly increases the degrees of freedom available for filter design. In particular, phase-only filters can be designed to yield the desired temporal intensity profile. An important example is the use of periodic phase-only spectral filters to produce high quality pulse trains.[47,48] As in Fig. 3, where spectral amplitude filtering is used for pulse train generation, the repetition rate of the pulse train is equal to the periodicity of the spectral filter. However, unlike the spectral amplitude filtering case, the envelope of the pulse train depends on the structure of the phase response within a single period of the phase filter. It turns out that by using pseudorandom phase sequences with sharp autocorrelation peaks (similar to those used in CDMA and other forms of spread spectrum communication)[49] as the building blocks of the phase filter, one can generate pulse trains under a smooth envelope. The intensity cross-correlation measurement of a resulting experimental pulse train with 4.0 THz repetition rate, generated using 75 fs input pulses and binary phase masks based on periodic repetitions of the so-called M (or maximal length) sequences,[49] is shown in Fig. 7(a).[47] The pulse train is clean, and the pulses are well separated. Pulse trains with similar intensity profiles (not shown) have been produced by spectral amplitude filtering, but with substantially reduced energies. Note that the optical phase is constant from pulse to pulse in trains produced by amplitude filtering, unlike the phase filtering case, where the optical phase varies. Pulse trains such as that in Fig. 7(a)

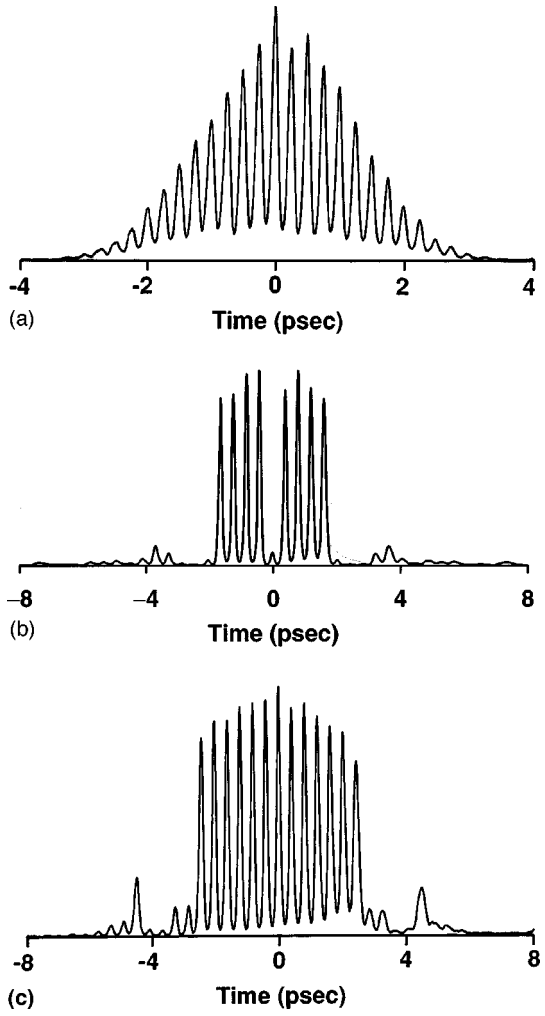

FIG. 7. Pulse trains generated by phase-only filtering. (a) Pulse train under a smooth envelope. (b) and (c) Pulse trains under a square envelope.

have been utilized for experiments demonstrating selective amplification of coherent optical phonons in crystals,[50,51] laser control over coherent charge oscillations in multiple quantum well semiconductor structures,[52,53] and enhancement of terahertz radiation emitted from photoconducting antennas.[54] Similar pulse trains have also been generated using input pulses below 20 fs, both with fixed masks[30] and with SLMs,[36] and with repetition rates in the vicinity of 20 THz.[36]

Pulse trains with different envelopes can be generated by varying the details of the phase response within a single period of the periodic phase filter.[47,48] For example, flat-topped pulse trains have been generated by using filters based on the so-called Dammann gratings.[55–57] Damman gratings are computer generated holograms that have previously been used to split an individual laser beam into an equally spaced, equal intensity array of beams in space. The structure for a Dammann grating consists of a periodic binary phase function, where the period of the phase modulation is selected to yield the desired beam separation in the spatial output array and the phase structure within a single modulation period is designed using numerical global optimization techniques to provide the desired number of beams, with as little energy as possible outside the target array area. In spatial optics, the output beam array can be obtained by passing a single input beam first through the Dammann grating and then through a lens, which takes the spatial Fourier transform. Pulse sequences in the time domain can be formed by placing similar masks at the Fourier plane of a pulse shaper. One example of time domain data, obtained by placing a binary phase mask fabricated according to a Dammann grating design into a femtosecond pulse shaper, is shown in Fig. 7(b). The waveform consists of a relatively uniform sequence of eight pulses, with one central pulse missing. Waveforms with the missing central pulse restored have been obtained by adjusting the phase difference on the mask to be less than π—see Fig. 7(c). These time domain results, achieved by using a phase filter originally designed for spatial beam forming applications, underscores again the close analogy between time domain and space domain Fourier optics.

It is worth noting that design of Dammann phase gratings for spatial array generation is usually accomplished through numerical optimization techniques. New phase-only filters designed to generate other femtosecond waveforms can also be found using numerical optimization codes. Several authors have employed simulated annealing algorithms to design either binary[48] or gray-level[58–60] phase-only filters, which were tested in pulse shaping experiments using either binary phase masks or liquid crystal modulators, respectively. Binary (0-π) phase filters produce waveforms with symmetrical intensity profiles, while gray-level phase filters (typically with four or more phase levels) can be used for generating pulse trains and other waveforms with asymmetric intensity profiles. We emphasize that phase-only filtering is generally sufficient only when the target time-domain waveform is not completely specified, e.g., when the time-domain intensity is specified but the temporal phases are left free.

C. Results from pulse shaping theory

It is important to have a quantitative description of the shaped output waveform $e_{\text{out}}(t)$. In terms of the linear filter formalism, Eqs. (2.1)–(2.4), we wish to relate the linear filtering function $H(\omega)$ to the actual physical masking function with complex transmittance $M(x)$. To do so, we note that the field immediately after the mask can be written

$$E_m(x,\omega) \sim E_{\text{in}}(\omega) e^{-(x-\alpha\omega)^2/w_0^2} M(x), \tag{2.7}$$

where $$\alpha = \frac{\lambda^2 f}{2\pi c d \cos(\theta_d)} \tag{2.8a}$$

and

$$w_0 = \frac{\cos(\theta_{\text{in}})}{\cos(\theta_d)} \left(\frac{f\lambda}{\pi w_{\text{in}}} \right). \tag{2.8b}$$

Here α is the spatial dispersion with units cm $(\text{rad/s})^{-1}$, w_0 is the radius of the focused beam at the masking plane (for any single frequency component), w_{in} is the input beam radius before the first grating, c is the speed of light, d is the grating period, λ is the wavelength, f is the lens focal length, and θ_{in} and θ_d are the input and diffracted angles from the first grating, respectively.

Note that Eq. (2.7) is in general a nonseparable function of both space (x) and frequency (ω). This occurs because the spatial profiles of the focused spectral components can be altered by the mask—e.g., some spectral components may impinge on abrupt amplitude or phase steps on the mask, while others may not. This leads to different amounts of diffraction for different spectral components and results in an output field which may be a coupled function of space and time. This space-time coupling has been analyzed by several authors.[61–63]

On the other hand, one is usually interested in generating a spatially uniform output beam with a single prescribed temporal profile. In order to obtain an output field which is a function of frequency (or time) only, one must perform an appropriate spatial filtering operation. Thurston *et al.*[64] analyze pulse shaping by expanding the masked field into Hermite–Gaussian modes and assuming that all of the spatial modes except for the fundamental Gaussian mode are eliminated by the spatial filtering. In real experiments the Gaussian mode selection operation could be performed by focusing into a fiber (for communications applications) or by coupling into a regenerative amplifier (for high power applications). This can be also be performed approximately by spatial filtering or simply by placing an iris after the pulse shaping setup. In any case, if one takes the filter function $H(\omega)$ to be the coefficient of the lowest Hermite–Gaussian mode in the expansion of $E_m(x,\omega)$, one arrives at the following expression:[27,64]

$$H(\omega) = \left(\frac{2}{\pi w_0^2} \right)^{1/2} \int dx\, M(x) e^{-2(x-\alpha\omega)^2/w_0^2}. \tag{2.9}$$

Equation (2.9) shows that the effective filter in the frequency domain is the mask function $M(x)$ convolved with the *intensity* profile of the beam. The main effect of this convolution is to limit the full width at half maximum (FWHM) spectral resolution $\delta\omega$ of the pulse shaper to $\delta\omega \cong (\ln 2)^{1/2} w_0/\alpha$.

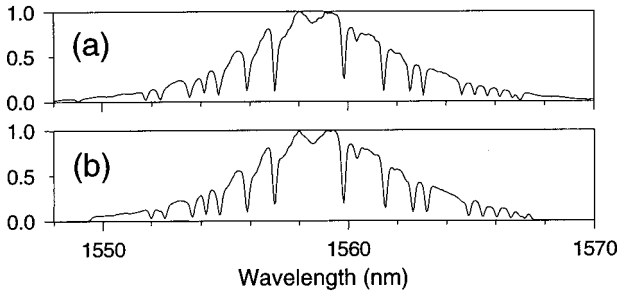

FIG. 8. Experimental (a) and theoretical (b) power spectrum resulting from spectral encoding using a pseudorandom binary phase code.

Physical features on the mask smaller than $\sim w_0$ are smeared out by the convolution, and this limits the finest features which can be transferred onto the filtered spectrum. One consequence of this picture is that wavelength components impinging on mask features which vary too fast for the available spectral resolution are in part diffracted out of the main beam and eliminated by the spatial filter. This can lead to phase-to-amplitude conversion in the pulse shaping process.[41,64,65] Conversely, in the limit $w_0 \rightarrow 0$, the apparatus provides perfect spectral resolution, and the effective filter is just a scaled version of the mask.

The effect of finite spectral resolution and phase-to-amplitude conversion is illustrated by Fig. 8(a).[41] The data show the power spectrum measured for a pulse spectrally encoded using a pseudorandom binary phase code in the context of a fiber optic CDMA communications experiment. The encoding process impresses a pseudorandom sequence of 31 phases, each either zero or π, onto the spectrum. Even though the code itself is phase-only, a series of dips is present in the encoded spectrum. Each dip corresponds to a phase jump in the spectral code and results from power diffracted out of the main beam which is not refocused into the output fiber. Figure 8(b) shows the theoretical spectrum, simulated on the basis of Eq. (2.9), the known phase code, and the appropriate values for α and w_0. The measured power lost in the encoding process was also compared with the simulation results as a function of code length.[41] For both the spectrum and the power lost, the agreement between experiment and simulation is excellent. These experiments, and others like them, show that Eq. (2.9) provides an appropriate theoretical description, including the effect of diffraction losses due to mask features, provided that a suitable spatial filter is employed following the pulse shaping apparatus.

Note that in our treatment earlier we assume that the output Gaussian mode which is selected is matched to the input mode. The case where the input and output mode sizes are not matched is analyzed in Ref. 66; in some cases this can give improvement in spectral resolution compared to that expected from Eq. (2.9).

The effect of finite spectral resolution can be understood in the time domain by noting that the output pulse $e_{\text{out}}(t)$ will be the convolution of the input pulse $e_{\text{in}}(t)$ with the impulse response $h(t)$. The impulse response in turn is obtained from the Fourier transform of Eq. (2.9) and can be written as follows:

$$h(t) = m(t)g(t), \tag{2.10a}$$

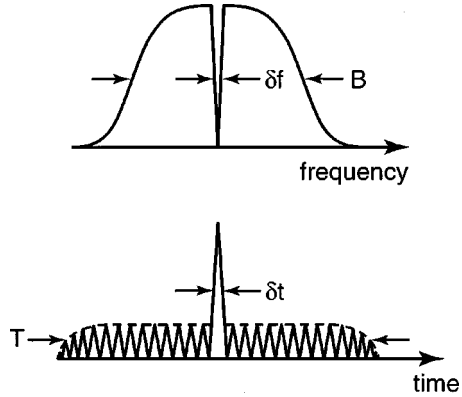

FIG. 9. Schematic time- and frequency-domain plots illustrating limits on the complexity of shaped pulses.

where

$$m(t) = \frac{1}{2\pi} \int d\omega\, M(\alpha\omega) e^{i\omega t} \tag{2.10b}$$

and

$$g(t) = \exp(-w_0^2 t^2 / 8\alpha^2). \tag{2.10c}$$

Thus, the impulse response is the product of two factors. The first factor $m(t)$ is the Fourier transform of the mask (appropriately scaled) and corresponds to the infinite-resolution impulse response. The second factor $g(t)$ is an envelope function which restricts the time window in which the tailored output pulse can accurately reflect the response of the infinite-resolution mask. The FWHM duration of this time window (in terms of intensity) is given by

$$T = \frac{4\alpha\sqrt{\ln 2}}{w_0} = \frac{2\sqrt{\ln 2}\, w_{\text{in}} \lambda}{cd \cos\theta_{\text{in}}}. \tag{2.11}$$

The time window is proportional to the number of grating lines illuminated by the input beam multiplied by the period of an optical cycle. A larger time window can only be obtained by expanding the input beam diameter. The shortest feature in the output shaped pulse is of course governed by the available optical bandwidth.

These results impose limits on the complexity of shaped pulses, which can be understood in terms of schematic frequency and time domain plots in Fig. 9. The shortest temporal feature that can be realized, δt, is inversely related to the total bandwidth $B(B\,\delta t \cong 0.44)$, and the maximum temporal window T is inversely related to the finest achievable spectral feature $\delta f(\delta f T \cong 0.44)$. Here T, Δt, B, and δf all refer to FWHMs. We define η as a measure of the potential complexity of the shaped pulse, as follows:

$$\eta = B/\delta f = T/\delta t. \tag{2.12}$$

Thus, η describes the number of distinct spectral features that may be placed into the available bandwidth, or equivalently, the number of independent temporal features that may be synthesized into a waveform. This measure is related to the maximum time-bandwidth product: $BT \cong 0.44\eta$. An expression for the complexity η is given in terms of the grating and input beam parameters as follows:

$$\eta = \frac{\Delta\lambda}{\lambda}\frac{\pi}{(\ln 2)^{1/2}}\frac{w_{\text{in}}}{d\cos(\theta_{\text{in}})}, \tag{2.13}$$

where $\Delta\lambda$ is the bandwidth (in units of wavelength).

We consider a numerical example. If we assume an 850 nm center wavelength, an 1800 line/mm grating, an incident angle of 50° (near Littrow), a 100 fs pulse, and $w_{\text{in}} = 2$ mm, the resultant time window and complexity are $T = 26.4$ ps and $\eta = 264$, respectively. These numbers are typical in that several experiments have demonstrated time windows on the order of tens of picoseconds and complexities of one hundred to a few hundred. Larger time windows are possible using larger input beams; higher complexities are possible using either larger input beams or shorter pulse widths or both. Pulse shaping time windows in the 100 ps range[67] have been reported, as have experiments with pulses as short as 13 fs.[36] However, in most cases the demonstrated pulse shaping complexity is still in the range of a few hundred or less. Note that Eqs. (2.11) and (2.13) are the upper bounds on the time window and complexity as set by fundamental optics. Achieving these limits depends on having a sufficient number of spatial features available in the pulse shaping mask or SLM; and for increasing complexities, the requirements on the precision of the pulse shaping mask and the optical system become increasingly stringent.

The earlier discussion, which results from an approximate treatment of diffraction at the mask, has been found to adequately describe a great number of experimental results. We reiterate, however, that these results are only valid when a suitable spatial filter is employed so that the pulse shape is constant across the spatial beam profile. Practically, it is also helpful to avoid using a masking function whose infinite resolution impulse response function exceeds the available time window.

Several papers have analyzed the space-time coupling effects arising due to diffraction from the pulse shaping mask.[61–63] Wefers and Nelson[62] have obtained a simple analytical expression which describes this space-time coupling. Assuming an input electric field proportional to $f_{\text{in}}(x)e_{\text{in}}(t)$, and assuming no aperturing or spatial filtering by the optical system (except at the mask!), the shaped electric field after the final grating is given by

$$e_{\text{out}}(x,t) \sim f_{\text{in}}(x+vt)\int dt' e_{\text{in}}(t')m(t-t'), \tag{2.14a}$$

where

$$v = \frac{cd\cos\theta_{\text{in}}}{\lambda}. \tag{2.14b}$$

The integral gives the shaped pulse which would be obtained in the perfect spectral resolution (infinite time window) limit—i.e., the convolution of the input pulse with the scaled Fourier transform of the mask. The $f_{\text{in}}(x+vt)$ multiplier represents a time-dependent spatial shift of the shaped waveform. It is interesting to note that for a spatial shift Δx along the output beam, the corresponding time offset is given by the number of grating grooves intercepted by the spatial shift $(\Delta x/d\cos\theta_{\text{in}})$ multiplied by the optical period (λ/c). Equation (2.14) does not explicitly include any time window. However, a time window automatically arises if one includes an aperture selecting a portion of the shaped beam. For a Gaussian input beam and a spatial filter which selects the matched Gaussian spatial mode of the shaped beam, one obtains the results in Eqs. (2.7)–(2.11).

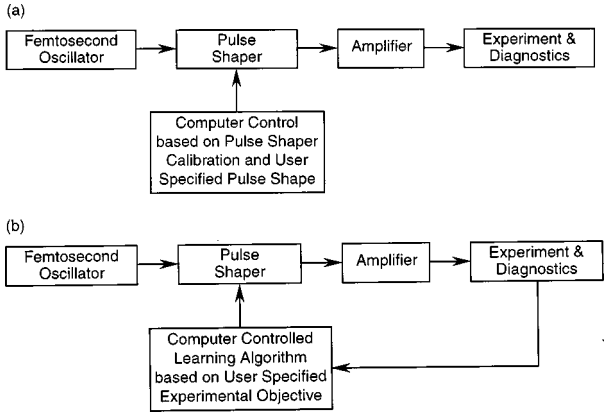

FIG. 10. Control strategies for femtosecond pulse shaping. (a) Open loop control. (b) Feedback or adaptive control. Note that these experiments can be performed either with or without the amplifier pictured in the figure.

D. Control strategies for pulse shaping

Femtosecond pulse shapers can be operated either under open loop control or in a feedback (adaptive control) configuration. These concepts are illustrated in Fig. 10. Note that a femtosecond amplifier system may optionally be included under either control strategy, depending on the experimental requirements.

Let us first consider the open loop configuration, Fig. 10(a). Here the desired output waveform is specified by the user, and reasonable knowledge of the input pulse is also usually available. Therefore, the desired transfer function is known, and one sets the pulse shaping SLM (in the case of programmable pulse shaping) to provide this transfer function. If there is additional linear distortion present between the input and output (e.g., phase aberration in a chirped pulse femtosecond amplifier), the pulse shaper can be programed so that its transfer function also includes precompensation for such distortion. This open loop strategy requires precise calibration of the SLM. However, precise characterization of the input pulse is often unnecessary, provided that the input pulse is known to be shorter than shortest features desired in the shaped output waveform. Open loop control, which has been used since the original pulse shaping experiments, is the only method applicable with fixed masks. It has been used to obtain high quality shaped pulses for many different experimental applications and remains in common use for programmable pulse shaping with SLMs.

The ability to program a pulse shaper under computer control has led recently to several interesting demonstrations of adaptive pulse shaping [Fig. 10(b)]—or pulse shaping under feedback control.[37,38,68–73] In these experiments one usually starts with a random spectral pattern programmed into the pulse shaper, which is updated iteratively according to a stochastic optimization algorithm based on the difference between a desired and measured experimental output. In this

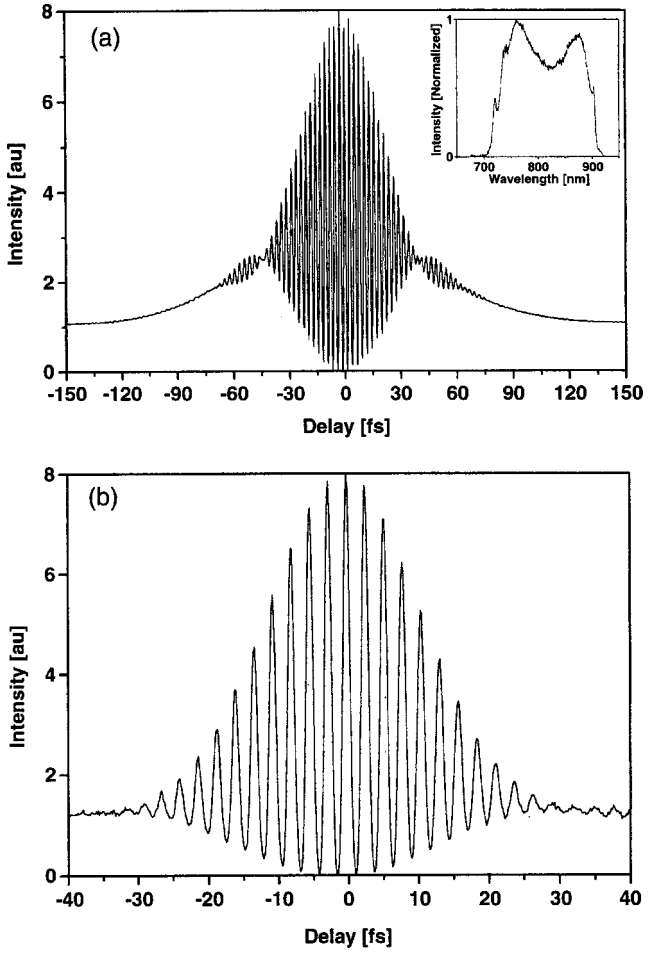

FIG. 11. Results from adaptive pulse shaping. (a) Interferometric autocorrelation measurement of highly chirped pulses from a Ti: sapphire laser. (b) Measurement of pulse compressed to nearly the bandwidth limit through adaptive pulse shaping. Inset: optical power spectrum.

way femtosecond waveform synthesis or chirp compensation can be achieved without the need to explicitly program the pulse shaper. Adaptive pulse shaping experiments have been performed using liquid crystal modulator arrays,[37,68–72] acousto-optic modulators,[73,74] and deformable mirror phase modulator arrays.[38] Experimental demonstrations have included chirp compensation and shaping of low energy pulses from femtosecond oscillators,[37,38,68,70] correction of residual chirps remaining after the pulse stretching-compression process in high energy chirped pulse amplifiers,[69,71] and quantum control experiments demonstrating adaptive pulse shape control of fluorescence yields[73] and photodissasociation products.[72] One example of data from an adaptive pulse compression experiment is shown in Fig. 11.[37] In this work a Ti:sapphire laser was deliberately misaligned in order to generate highly chirped output pulses [~80 fs, Fig. 11(a)], although the ~150 nm wide laser bandwidth (see inset) could potentially support sub-10 fs pulses. The state of a liquid crystal phase modulator array in a pulse shaper was adaptively controlled using a simulated annealing algorithm in order to maximize the average second harmonic signal measured after an external doubling crystal (the second harmonic is expected to be highest for the shortest, most intense pulse). The interferometric autocorrelation trace of the pulse obtained after 1000 iterations is shown in Fig. 11(b) (note the different time scale). The pulse is compressed to 14 fs, much closer to the bandwidth limit, and the pulse quality is greatly improved. The time required to run this experiment was roughly 15 min (~1 s per iteration).

In adaptive pulse shaping neither the input pulse (see earlier example) nor the calibration of the SLM nor the output laser waveform need to be specified. What does need to specified is the experimental outcome to be optimized and the adaptive learning algorithm to be employed. The adaptive control strategy can be appropriate when the calibration of the SLM is difficult or the state of the SLM depends in a complicated way on the input variables. It can also be particularly useful when the appropriate laser waveform is not known. One example is in the field of coherent control,[75] where shaped laser waveforms can be a tool for controlling quantum mechanical motions, with potential application, e.g., to laser controlled chemistry. In many real systems the Hamiltonian is not known with sufficient accuracy to predict the appropriate laser waveform. In these cases the adaptive approach can be used to search for the laser waveform which gives the best experimental result, such as optimizing the yield of a particular photochemical product.[76,77]

E. Pulse shaping in amplified systems

We comment briefly on pulse shaping in amplified femtosecond systems. Amplifiers are needed whenever modelocked oscillators alone are insufficient to produce shaped pulses at the desired energy levels. Briefly, the pulse shaper may be placed before the amplifier (as in Fig. 10), after the amplifier, or in some cases it may be part of the amplifier. In the late 1980s several experiments were reported in which high energy shaped pulses were generated by placing a pulse shaper containing fixed masks after a microjoule level amplifier system.[45,50,78,79] In recent experiments with millijoule level amplifier systems and programmable pulse shapers, the pulse shaper has been placed either before[80] or after[71,73] the amplifier. Placing the pulse shaper before the amplifier has the advantage that the danger of damage to the SLM is minimized. Furthermore, in the case of a saturated amplifier, the output energy is not strongly dependent on changes in the input energy; therefore, losses during the pulse shaping process before the amplifier need not result in substantially lower energies after the amplifier. One should note, however, that in the case of very high power amplifiers, one may need to consider the influence of pulse shaping on nonlinearities in the amplifier. In chirped pulse amplifiers, the pulse is stretched very substantially in order to lower the peak intensity and, hence, avoid nonlinearities in the amplifier. Chirping or stretching of a shaped pulse may in some situations modulate or otherwise influence the intensity seen by the amplifier, which may lead to nonlinear distortions in the amplified output waveform.[81] Note that since chirped pulse amplifiers contain grating based pulse stretchers and compressors, it is also possible to perform pulse shaping within the amplifier by placing a SLM at the appropriate point in the stretcher or compressor. This approach has been reported in Ref. 82, where a liquid crystal phase modulator array was

used within the stretcher to obtain millijoule level shaped pulses. However, this approach requires that the stretcher be constructed to match the aperture of the SLM, which cuts down on design flexibility which may be needed to achieve very large stretching ratios.

F. Pulse shaper alignment

The optical components within Fourier plane pulse shapers have many degrees of freedom, and careful alignment of the components is critical. A recipe for pulse shaper alignment, used in much of the author's work with fixed masks or liquid crystal SLMs, is given below. We assume the pulse shaper is assembled on a flat working surface, e.g., an optical table, and a short pulse source is used for the alignment.

(1) Make sure that the input beam from the laser is collimated and propagating in a plane parallel to the optical table surface.

(2) Align the first diffraction grating such that the plane of the grating surface and the rulings of the grating lie in a plane normal to the optical table. This can be achieved by observing the specular reflection (zero order diffraction) as well as the desired diffraction order and making sure that both propagate in a plane parallel to the table. With correct alignment the direction in which the optical frequency components spread should also be parallel to the table surface.

(3) Place the first lens approximately one focal length away from the first grating, with the lens centered on and normal to the diffracted beam. The height of the lens should be adjusted to ensure that the transmitted beam still propagates parallel to the table surface. However, the exact positioning of the lens is usually not critical.

(4) The mask or SLM can be placed at approximately the back focal plane of the first lens, making sure that the aperture of the SLM is centered on the spatially dispersed frequency spectrum. At this point the SLM should be set to its quiescent state (no amplitude or phase modulations). Alternately, the mask or SLM can be left out at this point and inserted after the rest of alignment is complete.

(5) Position the second lens two focal lengths away from the first lens. The lens should be translated closer to or further from the first lens until the transmitted beam is collimated. The height of the second lens is adjusted as per step (3).

(6) Position the second grating one focal length from the second lens. Adjust the tilt of the grating and the direction of the grating rulings in the same way as per step (2). There are then two further critical adjustments:

(6a) The rotation of the grating about the vertical axis must be set to exactly match that of grating one. This can be achieved by observing the output beam in the far field and making sure that there is no remaining spatial dispersion—i.e., all the frequency components should be optimally overlapped. To help visualize residual spatial dispersion, one can place a card in the masking plane and sweep it across the spatially dispersed frequencies. If there is residual spatial dispersion at the output, one can see an image of the card sweeping across the output beam; if there is no spatial dispersion, the output will be uniformly attenuated as the card is moved in the masking plane.

(6b) The distance between the second and first grating must be set for exactly four focal lengths in order to obtain zero group velocity dispersion. (In the case of a chirped input pulse, one may vary the grating separation from this condition in order to compensate the input frequency chirp.) The grating distance can be fine tuned by measuring the output pulse duration, for example, via intensity cross correlation using an unshaped pulse directly from the laser as a reference. The grating is translated until the output pulse width is minimized. In order to estimate how precisely the grating separation must be set, it is helpful to use the following formulas, which specify the grating dispersion as a function of grating separation:[42,83,84]

$$\frac{\partial^2 \phi(\omega)}{\partial \omega^2} = \frac{\lambda^3 (L-4f)}{2\pi c^2 d^2 \cos^2 \theta_d} \tag{2.15a}$$

and equivalently

$$\frac{\partial T(\lambda)}{\partial \lambda} = \frac{\lambda (L-4f)}{c d^2 \cos^2 \theta_d}. \tag{2.15b}$$

Here $\phi(\omega)$ is the spectral phase and $T(\lambda)$ is the wavelength dependent group delay. L-$4f$ represents the detuning of the grating separation from the dispersion-free $4f$ separation condition. The grating separation should be set so that T varies by much less than one pulse width across the bandwidth of the pulse $\Delta\lambda$, or equivalently so that ϕ varies by much less than π.

(7) Now the pulse shaping SLM can be activated [inserted first if not done in step (4)]. Its aperture should be centered on the desired spectral region, and it should be placed at the back focal plane of the first lens where individual frequency components are focused to their minimum size. Both adjustments are facilitated by monitoring the output spectrum from the pulse shaper in order to observe the features placed by the mask or SLM onto the spectrum.

G. Measurement of shaped pulses

The task of producing a shaped ultrashort pulse is closely connected to the task of measuring such shaped pulse. The field of ultrashort pulse shape measurement has undergone dramatic progress during the last decade, in parallel with progress in pulse shaping. Although it is not possible within the scope of this article to give a comprehensive discussion of pulse measurement techniques, nevertheless, in the following we do give a brief, nonexhaustive overview of methods which have been most frequently applied to characterization of shaped pulses.

The technique which has been most often used for measuring shaped pulses (especially until recently) is intensity cross correlation, which yields a signal

$$X_I(\tau) \sim \int dt\, I_1(t-\tau) I_2(t). \tag{2.16}$$

This quantity can be obtained by measuring the average second harmonic power generated through the interaction of two pulses with intensity profiles $I_1(t-\tau)$ and $I_2(t)$ in a

second harmonic generation crystal as a function of the relative delay τ. When I_1 is a short pulse directly out of a modelocked laser, and I_2 is a shaped pulse significantly longer than I_1, then the cross-correlation signal $X_I(\tau)$ provides a good approximation to the shaped intensity profile. However, any very rapid features in I_2 varying on the same time scale as I_1 will be broadened. Furthermore, no phase information is available. Note, however, that if pulse shaping is successful in accurately generating a complicated desired intensity profile, as verified by intensity cross correlation, then one can usually infer that the desired phase profile is also generated at least reasonably well, even without direct measurement. This proved true, e.g., in dark soliton propagation experiments, where the nonlinear propagation of the dark soliton pulse in an optical fiber was sensitive both to the shaped pulse intensity and phase profile.[78] Nevertheless, the lack of any direct phase information is a significant limitation of the intensity cross-correlation method.

Unshaped pulses in ultrafast optics have been measured for many years via intensity autocorrelation (see for example Ref. 85), which is obtained from Eq. (2.16) by setting $I_1(t) = I_2(t)$. Although the exact pulse shape cannot be determined from intensity autocorrelation data, for simple pulse shapes the approximate pulse duration can still be obtained. However, for complicated shaped pulses, the intensity autocorrelation is usually not useful since most pulse shape information is lost.

In addition to intensity cross correlation, field cross-correlation measurements can also be useful, especially for low power signals. The electric field cross correlation is given by

$$X_e(\tau) \sim \int dt\, e_1(t-\tau) e_2^*(t) + \text{c.c.}, \tag{2.17}$$

where ''c.c.'' means complex conjugate. This quantity can be obtained by recording the interference fringes between two field $e_1(t-\tau)$ and $e_2(t)$ as a function of delay τ at the output of an interferometer. If $e_1(t)$ is a short reference pulse (e.g., right out of the laser) and $e_2(t)$ is a longer shaped pulse, then the interference envelope provides an approximate measurement of the shaped electric field amplitude $|e_2(t)|$. If the phases of the fringes are also carefully measured, then one can also determine the time-dependent phase of $e_2(t)$. In this way the shaped electric field is completely characterized.

An important breakthrough in the field of ultrafast optics was the relatively recent development of techniques for complete amplitude and phase characterization of ultrashort pulses. The best known of these techniques is called frequency-resolved optical gating, or FROG.[86,87] In FROG one gates the pulse to be measured with an identical time-delayed version of itself. Various gating mechanisms, such as second harmonic generation, nonlinear polarization rotation, and transient gratings, have been employed. The power spectrum of the output pulse resulting from the nonlinear gating interaction is measured with a spectrometer as a function of time delay between the two pulses. In the case of the polarization rotation gating mechanism, the measured quantity $S(\omega,\tau)$ can be expressed as

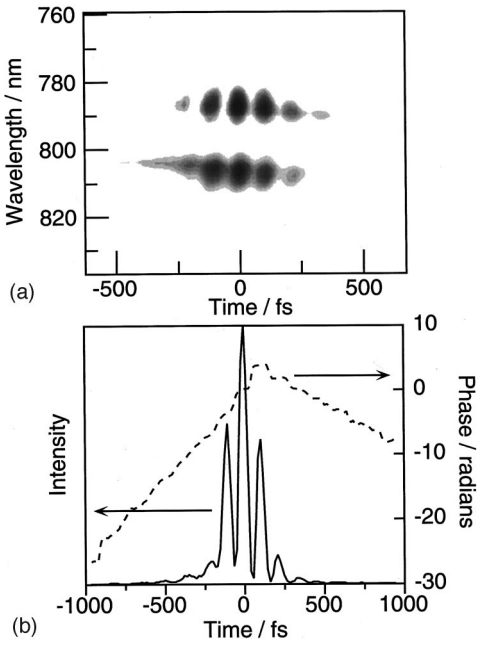

FIG. 12. (a) Measured FROG trace of amplified, shaped signal, (b) Time-dependent intensity (solid) and phase (dashed) retrieved from FROG data.

$$S(\omega,\tau) \sim \left| \int e_{\text{in}}(t) |e_{\text{in}}(t-\tau)|^2 e^{-j\omega t} dt \right|^2, \tag{2.18}$$

where $e_{\text{in}}(t)$ is the pulse to be characterized. Equation (2.18) is a kind of spectrogram, a type of time-frequency transform which is well known in speech analysis for example. One important feature of this measurement approach is that time dependent frequency shifts (chirps) can often be visualized directly and intuitively. A second (and most important) feature is that both the complete intensity and phase profiles of the ultrashort pulse can be recovered, in practice by using iterative computer optimization techniques.

One example of FROG data, using polarization rotation gating, is shown in Fig. 12.[87,88] Here the input pulses were derived from a Ti:sapphire chirped pulse regenerative amplifier, with a mask placed at the Fourier plane of the pulse stretcher in order to block the central frequency components as a simple example of pulse shaping. The modulation along the delay axis in the experimental FROG trace [Fig. 12(a)] is indicative of a strong temporal modulation, which is in fact observed in the retrieved multiple-pulse intensity profile [Fig. 12(b)]. The modulation along the wavelength axis of the FROG trace arises due to the double peaked nature of the shaped spectrum.

A second example of FROG data, applied to optimization of high power pulses from a chirped pulse amplifier system though pulse shaping, is presented in Sec. VIII C (Fig. 31).

There are two ways in which FROG can be applied for characterization of shaped pulses. In the first, FROG is applied to measure the shaped pulse itself, as in the example above. A limitation of this approach is that for sufficiently complicated waveforms, convergence of the computer routine for recovering the temporal phase and intensity profiles from the FROG data may become less dependable. Some

examples of waveforms from a pulse shaper that have been characterized by FROG are published in Refs. 88–90. In the second case, FROG is used to completely characterize pulses from the modelocked laser, which then serve as reference pulses for measurement of the more complicated shaped pulses, using noniterative techniques such as intensity or electric field cross correlation or spectral interferometry (see later).

Another technique which can be applied to characterization of shaped pulses is based on spectrally and temporally resolved upconversion. Experiments of this type split the waveform to be characterized into two parts: one is used as a reference, while the other is spectrally sliced, e.g., by using a simple pulse shaper containing a narrow slit at the Fourier plane or by using an interference filter, and thereby stretched in time to a duration much longer than the reference pulse. The upconversion cross-correlation signal between the reference and spectrally sliced pulses is generated using a second harmonic crystal and then analyzed. In the earliest approach the temporal position of the spectrally sliced pulse is measured as a function of the frequency of the transmitted spectrum, which is varied by translating the slit in the pulse shaper in a series of correlation scans.[91,92] This yields the frequency dependent delay $\tau(\omega)$, which is related to the spectral phase $\phi(\omega)$ by

$$\tau(\omega) = -\frac{\partial \phi(\omega)}{\partial \omega}. \tag{2.19}$$

In another approach, the upconversion signal was spectrally resolved using a spectrometer as a function of cross-correlation delay for a fixed position of the slit (i.e., a fixed spectral slice),[93] which gives similar information. Compared to FROG, one advantage of these techniques is that due to their noniterative nature, data can be analyzed fast enough for real-time display of the pulse characterization data. A disadvantage is that the bandwidth of the spectral slicer must be consciously chosen to be narrower than the most rapidly varying spectral features of the waveform under test (and this may not be known *a priori*) in order to achieve accurate results.

These early experiments cited earlier were used for characterization of unshaped pulses. Recently related methods have been applied to shaped pulses. In one case the method of Refs. 91 and 92 was generalized by including a multiple-slit mask in the Fourier plane.[44] Different pairs of slits give rise to various interference features in the time-domain intensity cross-correlation trace, and the temporal phase or position of these interference features provide information on $\phi(\omega)$, which can be extracted automatically via Fourier analysis. An improvement compared to the earlier work is that only a single cross-correlation scan is required. Two examples of pulse measurement data obtained using this so-called ''direct optical spectral phase measurement'' (DPSOM) are shown in Fig. 13. In one case an ''odd pulse'' [28] is generated by imposing an abrupt π phase shift into half of the spectrum, resulting in a pulse doublet which is partially resolved in the conventional intensity cross-correlation trace [Fig. 13(a)]. In the second case, a glass plate was inserted into half of the spectrum in the pulse shaper, leading to a

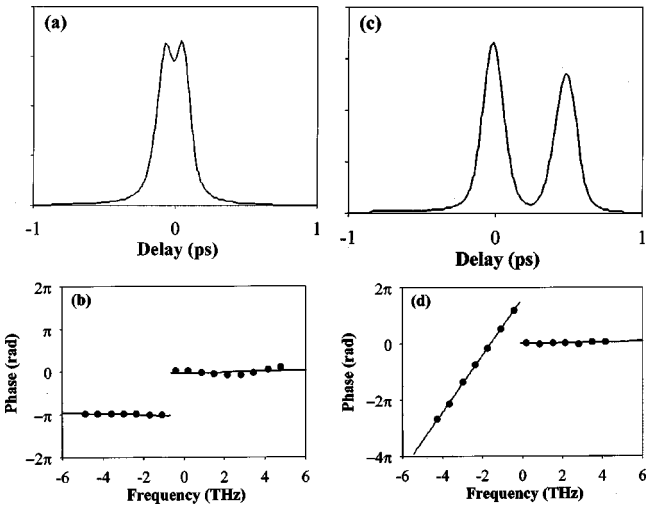

FIG. 13. (a) Intensity cross-correlation measurement and (b) spectral phase of femtosecond ''odd'' pulse. (c) Intensity cross-correlation measurement and (d) spectral phase of frequency shifted pulse doublet.

frequency-shifted pulse doublet, with the two pulses clearly resolved in the cross correlation [Fig. 13(c)]. The spectral phase data extracted from the DPSOM measurement are shown in Figs. 13(b) and 13(d). In the latter trace, the linear spectral phase evident over half of the spectrum corresponds as expected to a simple time delay of that half of the spectrum, as per Eq. (2.19).

Another case of this type of measurement which has been used for shaped pulse characterization has been named STRUT (for ''spectrally and temporally resolved upconversion technique''). This method is related to that of Ref. 93, but adapted for a single-shot measurement geometry and real-time data analysis for application to femtosecond amplifier systems.[94,95] An example of STRUT data is discussed in Sec. IV.

Finally, we mention spectral interferometry,[96] in which a short reference pulse with spectrum $E_1(\omega)$ is combined with the pulse to be characterized (e.g., a shaped pulse) with spectrum $E_2(\omega)$. The two pulses are given a relative time delay τ, and the resulting power spectrum is measured, which contains an oscillatory term of the form

$$S(\omega) \sim E_1(\omega) E_2^*(\omega) e^{-j\omega\tau} + \text{c.c.} \tag{2.20}$$

The spectrum contains fringes with period approximately τ^{-1}, which can be analyzed for the case of a short, bandwidth-limited (or well characterized) reference pulse to yield the complex spectrum $E_2(\omega)$. Note that it is the frequency dependent deviation of the spectral fringe period from the average period that yields spectral phase information; the average fringe period itself depends only on the relative delay and not on details of the pulse shape. Furthermore, since this is an interferometry technique, what is actually measured is the relative spectral phase of the pulse under test with respect to the reference pulse. Spectral interferometry has been used by several groups for characterization of shaped ultrashort pulses;[38,97–99] this technique is relatively easy to apply since a short pulse directly from the laser is usually available in pulse shaping experiments. In order to obtain the exact spectral phase of the pulse under test, one

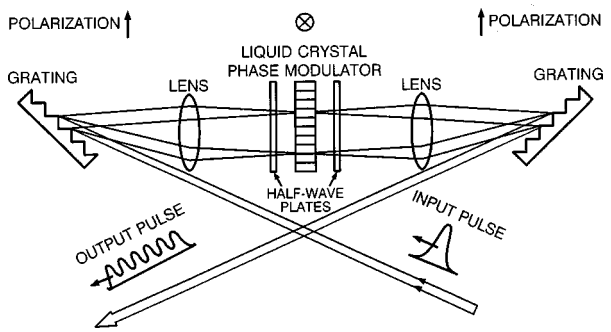

FIG. 14. Programable pulse shaping apparatus based on a LCM array.

must carefully characterize the reference pulse, e.g., by using FROG, as noted earlier.[87] On the other hand, if the reference pulse is already known to be approximately bandwidth limited, then one can get the approximate spectral phase of the shaped pulse without characterizing the reference pulse. The accuracy of this approach of course depends on how good the reference pulse is. However, in some situations one is only interested in characterizing the relative spectral phase between shaped and reference pulses; the exact form of the shaped pulse is not of interest, and therefore, the phase of the reference pulse is not relevant. This situation applies for example when one uses spectral interferometry to measure the dispersion of an optical component or subsystem placed in one arm of an interferometer. This approach has been used for characterization of a pulse shaper response to broadband incoherent light illumination[100] and for characterization of dispersion-compensated fiber links suitable for nearly dispersion-free femtosecond pulse transmission.[101]

III. PROGRAMMABLE PULSE SHAPING USING LIQUID CRYSTAL SLMs (LC SLMs)

We now proceed to discuss programmable pulse shaping using LC SLMs as a programmable mask. Pulse shaping using other programmable mask technologies, such as acousto-optic modulators, will be discussed in subsequent sections. Note that some of the discussion in this section, such as SLM construction, is specific to pulse shaping using LC arrays, whereas other aspects of the discussion, e.g., pulse shaping using phase-only filtering, cover concepts that are also applicable to pulse shaping using other SLM technologies.

A. Pulse shaping using electronically addressed liquid crystal modulator arrays

Liquid crystal modulator (LCM) arrays have been primarily configured for either phase-only or phase-and-amplitude operation in pulse shaping applications. Figure 14 depicts an apparatus for programmable pulse shaping using a LC SLM in phase-only operation.[34,35] Compared to pulse shaping setups using fixed masks, the main differences are that the fixed masks are replaced by the LC SLM, and a pair of half-wave plates are used to rotate the polarization in order to match that required by the modulator array. The LC array allows continuously variable phase control of each separate pixel (whereas fixed masks usually provide only binary phase modulation) and allows programmable control of the pulse shape on a millisecond time scale.

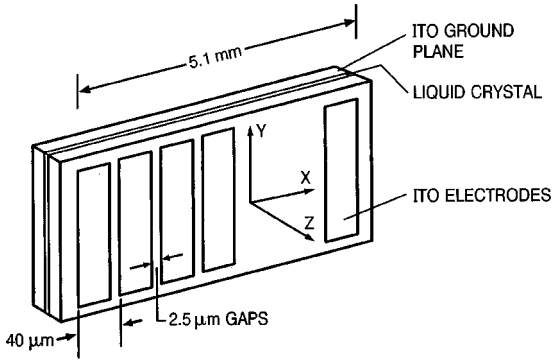

FIG. 15. Schematic diagram of an electronically addressed, phase-only LC SLM.

Figure 15 shows a schematic of an electronically addressed, phase-only LC SLM.[35] A thin layer of a nematic liquid crystal is sandwiched between two pieces of glass. The nematic liquid crystal consists of long, thin, rod-like molecules, which in the absence of an electric field are aligned with their long axes along the *y* direction. When an electric field is applied (in the *z* direction), the liquid crystal molecules tilt along *z*, causing a refractive index change for *y*-polarized light. A maximum phase change of at least 2π is required for complete phase control. In order to apply the required electric field, the inside surface of each piece of glass is coated with a thin, transparent, electrically conducting film of indium tin oxide. One piece is patterned into a number of separate electrodes (or pixels) with the corresponding fan out for electrical connections. In the original ''homemade'' modulator array in Fig. 15, there are 128 pixels with 40 μm center-to-center pixel spacing, 2.5 μm gaps between pixels, and a total aperture of 5.1 mm. Current commercially available LC SLMS also have 128 pixels, but with 100 μm center-to-center pixel spacing for a 12.8 mm aperture. The modulator array is controlled by a special drive circuit which generates 128 separate, variable amplitude signals to achieve independent, gray-level phase control of all 128 modulator elements. An additional point concerning the drive circuitry is worth noting. Each drive signal actually consists of a variable amplitude bipolar square wave, typically at a few hundred hertz or above, rather than a variable amplitude direct current (dc) level. The use of an alternating current (ac) drive signal is required to prevent electromigration effects in the liquid crystal.[102] Otherwise the use of a square wave as opposed to a dc level does not change the operation of the modulator, since the rotation of the liquid crystal molecules depends only on the amplitude (not the sign) of the applied voltage. Input data for the drive circuit is loaded into local memory from a personal computer, thus facilitating the generation of complex phase patterns.

Figure 16 shows an example of real-time pulse shaping data measured using an earlier 32 element liquid crystal phase modulator array and 75 fs pulses at 0.62 μm from a coliding-pulse-modelocked dye laser.[34] In the experiment half of the pixels were connected to a constant amplitude drive signal, while the other half were switched at a 20 Hz rate between the different drive levels. In one state, the phases are all the same, and the output is a single pulse

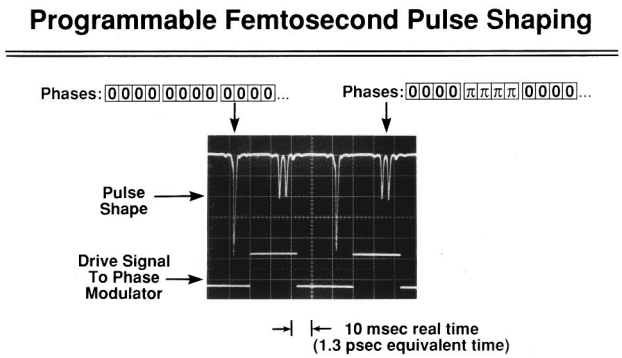

FIG. 16. Real-time pulse shaping data. Top trace: pulse intensity profiles measured using a real-time cross-correlation setup, showing switching between two distinct waveforms with 25 ms. Bottom trace: Time-varying drive signal to the LCM array.

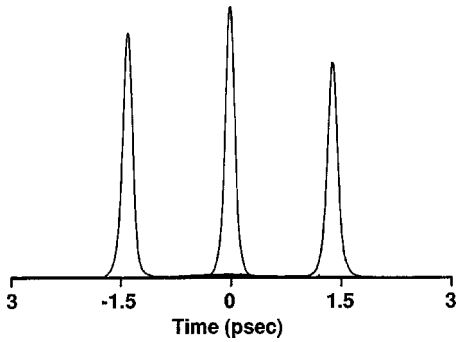

FIG. 17. Measurements of temporally shifted pulses achieved by placing linear phase ramps onto the spectrum. Data are shown for phase changes per pixel of 0 and $\pm\pi/4$, resulting in delays of 0 and ± 1.38 ps, respectively.

similar to the input pulse. In the other state, half of the pixels experience a relative phase shift of π. With the particular set of connections chosen in this experiment, this results in a pulse doublet. The pulse intensity profiles (top trace) shown in Fig. 16 were obtained by using a real-time cross-correlation setup, which was driven in synchronism with the time-varying drive signal (bottom trace). The data demonstrate complete switching from a single pulse to a pulse doublet within 25 ms. Under appropriate drive conditions, such LCM arrays are capable of switching in $\sim$10 ms. It is important to point out, however, that switch-on and switch-off times are usually not the same and depend on the bias voltage levels.

In order to use LC SLMs for gray-level phase control, a careful phase versus voltage calibration is required. This can be accomplished by using the array as an amplitude modulator for a continuous-wave (cw) laser. The laser is linearly polarized, with its polarization rotated 45° relative to the alignment direction of the liquid crystal, and focused onto a single pixel of the multielement modulator. The phase calibration is obtained by measuring the transmission through a subsequent crossed polarizer and using the relation

$$T(V) = \sin^2\left(\frac{\phi_y(V) - \phi_x}{2}\right), \tag{3.1}$$

where $T(V)$ is the fractional transmission through the crossed polarizer, and V is the applied voltage. Here ϕ_x corresponds to light polarized along the short axis of the liquid crystal molecules and is independent of the applied voltage. $\phi_y(V)$ corresponds to the voltage-dependent phase placed onto the optical spectrum when the modulator is positioned within the pulse shaper. In Ref. 35 several calibration curves were measured at different points along the array. The results shows good uniformity, as required for high quality pulse shaping. The LC array can also be calibrated *in situ* within the pulse shaper by using pulse characterization techniques such as spectral interferometry to measure the spectral phase changes imposed on an ultrashort pulse.

Gray-level phase control can be used to accomplish a number of interesting pulse shaping tasks. For example, using the modulator array to impart a linear phase sweep onto the spectrum corresponds in the time domain to pulse position modulation. Pulse position modulation relies on the fact that if $f(t)$ and $F(\omega)$ are a Fourier transform pair, then the delayed signal $f(t\text{-}\tau)$ is the Fourier transform of $F(\omega) \times \exp(-i\omega\tau)$. Thus, a pulse can be retarded (or advanced) by imposing a linear phase sweep onto its spectrum. The delay τ is given by the relation

$$\tau = -\delta\phi/2\pi\delta f, \tag{3.2}$$

where $\delta\phi$ and δf are, respectively, the imposed phase change per pixel and the change in optical frequency from one pixel to the next. For the experiments in Ref. 35 with a 128 element modulator, δf was approximately 0.092 THz, and therefore $\tau = -10.87\,(\delta\phi/2\pi)$ ps. The modulator was set to provide the required phase sweep modulo 2π, so that for each pixel the phase is in the range 0–2π. Figure 17 shows cross-correlation measurements of temporally shifted pulses achieved by means of pulse position modulation. Data are shown for a phase change per pixel ($\delta\phi$) of 0 and $\pm\pi/4$. The output pulses occur at 0 and ± 1.38 ps, in close agreement with Eq. (3.2). These data demonstrate the ability to shift the pulse position by many pulse widths by using spectral phase manipulation. Note that the total phase sweep in these experiments is 32π. Because pixellated LCM arrays can be programed to provide the desired phase function modulo 2π, large phase sweeps can be achieved using modulators with maximum phase changes as small as 2π. However, in any case of a smoothly varying target phase function, as here, the phase change from one pixel to the next should remain small enough that the staircase phase pattern, which is achieved by the LCM with its discrete pixels, is a sufficiently good approximation to the desired phase function. This point is discussed further in connection with Eq. (3.4) later.

Gray-level phase control can also be used to achieve programmable compression of chirped optical pulses.[34,35] As one example, we discuss recent experiments in which a pulse shaper equipped with a LC SLM was used to complement fiber dispersion compensation techniques in propagating $\sim$500 fs pulses over a 2.5 km optical fiber link.[40] The link consisted of 2.1 km of standard single-mode fiber (SMF) and 0.4 km of dispersion compensating fiber (DCF). Since SMF and DCF have dispersion with opposite signs at the operating wavelength of 1.56 μm, the fiber lengths can be adjusted to cancel all of the lowest order dispersion (i.e., phase varying

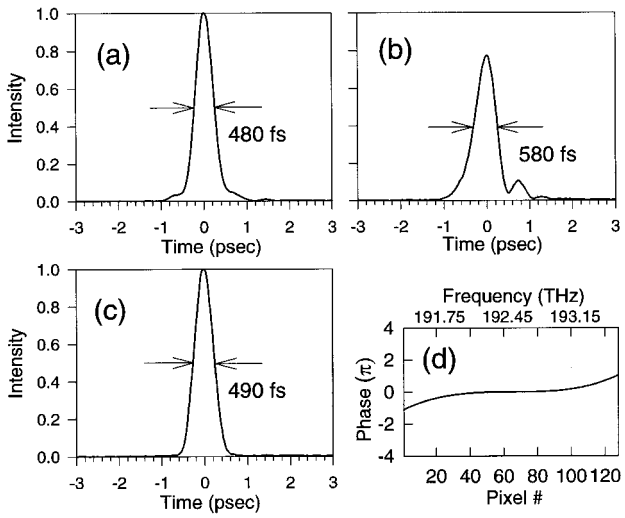

FIG. 18. (a) Input pulse to the 2.5 km fiber link. (b) and (c) Output pulses from the fiber link with (b) constant phase or (c) cubic phase correction applied to the LCM. (d) The cubic phase correction function.

quadratically with frequency). In addition, since the derivatives of the dispersion with respect and frequency also have opposite signs, the dispersion slope (i.e., cubic spectral phase variations) can also be partially compensated. In the experiments in Ref. 40, ~500 fs input pulses are first broadened ~400 fold in propagating through the SMF, then recompressed by the DCF to within a factor of 2 of the input pulse duration. Intensity cross-correlation measurements of the input pulse and output pulse after 2.5 km fiber propagation are shown in Figs. 18(a) and 18(b), respectively. The remaining broadening and distortion of the output pulse are characteristic of a cubic spectral phase variation. At this point, a LC SLM in a pulse shaper can be used to apply a spectral phase function [Fig. 8(d)] which is equal and opposite to the estimated residual phase variation of the output pulse from the fiber link. The result, shown in Fig. 18(c) is a completely recompressed pulse with the original pulse duration and no observable distortion. Thus, in these experiments all-fiber techniques are used for coarse dispersion compensation, while a programmable pulse shaper is used to fine tune any remaining dispersion. Similar experiments extended to shorter pulses (400 fs) and longer fiber spans (10 km) have recently been reported.[103] Pulse shapers with LCM arrays have also been used for compensation of residual dispersion in chirped pulse amplifier systems[69,82] and for adaptive compression of chirped pulses (see Sec. II D).

Gray-level phase control for pulse position modulation and programmable pulse compression, first demonstrated using LCMs, has also been extended to pulse shaping systems using moveable or deformable mirrors or acousto-optic modulators. This will be discussed in later sections.

LC SLMs have also been used for phase-only filtering and shaping of pulses with temporal resolution approaching 10 fs. Figure 19[36] shows one example, where ~13 fs pulses from a modelocked Ti:sapphire laser with a center wavelength of approximately 800 nm are shaped using an all-reflective-optics[30] pulse shaper. The LCM imparts a cubic spectral phase variation, leading to an asymmetric distortion

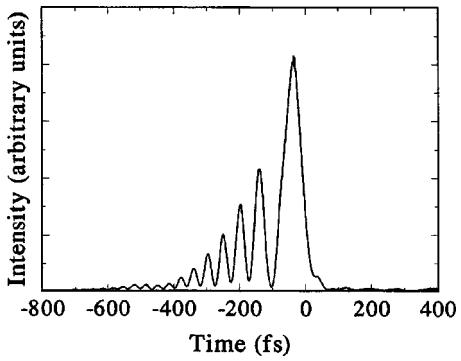

FIG. 19. Shaping of 13 fs pulses using a phase-only liquid crystal phase modulator array. In this example, the LCM produces a cubic spectral phase variation, leading to the asymmetric distortion seen in the intensity cross-correlation plot.

similar to that seen in Fig. 18(b) and in good agreement with the calculated pulse shape.[36]

For the most general pulse shaping operation, independent control of spectral phase and amplitude is desired. Given the appropriate input polarization relative to the liquid crystal axis, a single LCM array together with a polarizer can be used as an amplitude modulator; however, this leads also to a phase modulation which depends on the amplitude modulation level. Therefore, for independent phase and amplitude control the use of two LC arrays is required. Originally this was accomplished by modifying the setup of Fig. 14 to contain two telescopic lens pairs (four lenses) between the gratings, with separate LC SLMs between the first and second and third and fourth lenses, respectively.[58] A considerably simplified and improved setup, which is currently the preferred geometry for independent phase-amplitude modulation, was achieved by combining two LC arrays into a single device, as depicted in Fig. 20.[104] The two arrays are attached permanently with their pixels aligned and angular orientations fixed. Each array consists of 128 pixels on 100 μm centers with 3 μm gaps. The dual-LC–SLM unit is placed between a pair of Polacor polarizers passing light po-

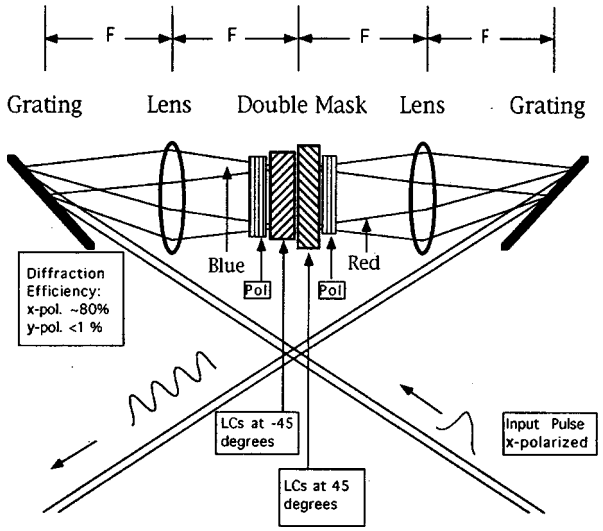

FIG. 20. Schematic diagram of pulse shaping using an electronically programmable dual LCM array offering independent phase and amplitude control.

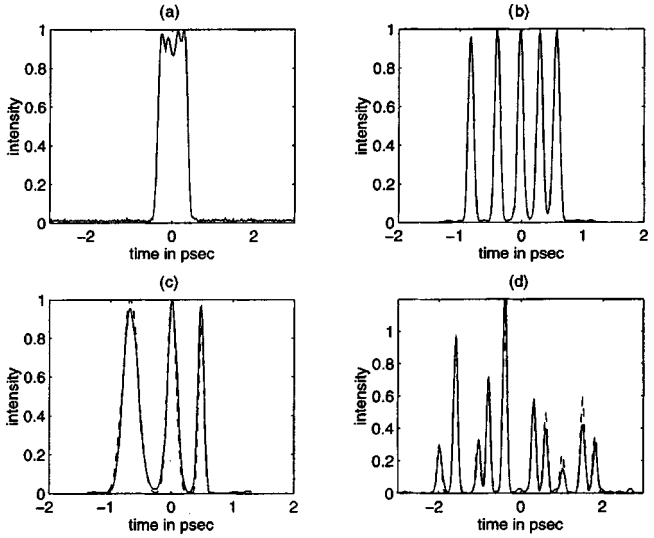

FIG. 21. Intensity cross-correlation traces of shaped pulses using the dual LCM array. (a) 800 fs square pulse. (b) Sequence of five, equal-amplitude pulses. (c) Three pulse sequence with different chirp rates per pulse. (d) Ten pulse sequence with pulse timing, amplitude, and phase control. In (c) and (d), the target intensity profiles are also shown (dashed lines). [With permission, from the Ann. Rev. Phys. Chem. **46** (1995), by Annual Reviews http://www.AnnualReviews.org]

larized along the spectral dispersion direction (horizontal in Fig. 20, denoted x). In this orientation there is no need to rotate the polarization between the gratings and LCM array; therefore, no wave plates are required. With the propagation direction denoted z and the second transverse direction (vertical in Fig. 20) denoted y, the long axes of the liquid crystal molecules in the two SLMs are aligned at $\pm 45°$ with respect to the x axis. When a voltage is applied to a pixel in one of the SLMs, the liquid crystal molecules in that pixel are rotated toward z, resulting in a phase modulation for the component of light parallel to the liquid crystal axis in that SLM.

For x-polarized light incident on a particular pixel of the dual SLM array, the output field is given by

$$\mathbf{E}_{\text{out}} = \frac{E_{\text{in}}}{2}\left\{ \exp(j\Delta\phi^{(1)})(\mathbf{x}+\mathbf{y}) + \exp(j\Delta\phi^{(2)})(\mathbf{x}-\mathbf{y}) \right. \tag{3.3a}$$

$$\left. = E_{\text{in}} \exp\left[\frac{j(\Delta\phi^{(1)}+\Delta\phi^{(2)})}{2}\right]\left[\mathbf{x}\cos\left(\frac{\Delta\phi^{(1)}-\Delta\phi^{(2)}}{2}\right) + j\mathbf{y}\sin\left(\frac{\Delta\phi^{(1)}-\Delta\phi^{(2)}}{2}\right)\right]\right\}, \tag{3.3b}$$

where E_{in} is the amplitude of the incident $\mathbf{x}$-polarized light and $\Delta\phi^{(1)}$ and $\Delta\phi^{(2)}$ are the voltage dependent birefringences of the first and the second LCM array, respectively. Using an output polarizer along $\mathbf{x}$, the output phase and attenuation can be set independently by controlling $\Delta\phi^{(1)}+\Delta\phi^{(2)}$ and $\Delta\phi^{(1)}-\Delta\phi^{(2)}$, respectively. Note that each LCM array in the dual SLM can be calibrated by measuring its amplitude modulation response as a function of voltage, with the other LCM array held at constant voltage.

Figure 21[105] shows four examples of pulse shaping using the dual LC SLM array. The input pulses were 70 fs in duration at 800 nm, and all the traces are intensity cross-correlation measurements using unshaped reference pulses directly from the laser. The data represent (a) an 800 fs square pulse, (b) a five pulse sequence of equal amplitude pulses in which both the pulse timings and phases are specified, (c) a three pulse sequence with different chirp rates per pulse, and (d) a sequence of ten 70 fs pulses with pulse timings, phases, and amplitudes all specified. In Figs. 21(c) and 21(d), the desired intensity profiles are also shown (as dashed lines). Clearly, waveforms with a rather high degree of complexity can be generated with excellent fidelity.

Finally, we note that dual LC SLMs may be useful for controlling the time-dependent polarization profile of ultrashort pulses. This possibility, as well as a simple experimental demonstration, are discussed in Ref. 104. Note, however, that the diffraction efficiency of the gratings, which usually have a strong polarization sensitivity, make polarization pulse shaping more difficult.

It is worth commenting on the degree of extinction possible with a LCM for pulse shaping. In my own group, we have sometimes used single layer LC SLMs (usually used for phase-only applications) as an amplitude only modulator, which is achieved by rotating the input polarization by 45° and using an appropriately oriented output polarizer. In the data of Ref. 106, an on-off ratio exceeding 30 dB is achieved for a commercial single layer LC SLM working in the 1.55 μm band. We also have experience using phase-amplitude LCMs at 1.55 μm, and are able to achieve on-off ratios in the range 25–30 dB.[107] In both cases, an accurate calibration of the LCM response is essential. In our experience we can achieve the best accuracy when the calibration is performed with the LCM placed inside the pulse shaper at exactly the position where it will be used.

The pixellation of electronically addressable phase or phase-and-amplitude LC SLMs leads to one significant limitation—namely, the SLM can only produce a staircase approximation even when a smooth spectral profile is desired. The requirement that the actual spectral modulation should approximate a smooth function despite the fixed, finite size of the individual modulator elements, limits the temporal range over which pulse shaping can be successfully achieved. Essentially this is a sampling limitation: the spectrum must vary sufficiently slowly that is adequately sampled by the fixed modulator elements. For the case of pulse position modulation, for example, we require $|\delta\phi| \ll \pi$, where $\delta\phi$ is the phase change per pixel. From Eq. (3.2), then, we find $|\tau| \ll 1/2\delta f$ (where δf is the optical frequency span corresponding to a single pixel). The effect of pixelation for pulse shaping in general has been analyzed in Ref. 35. The result is

$$e_{\text{out}}(t) \sim \left[e_{\text{in}}(t) * \sum_n h(t - n\delta f^{-1}) \right] \text{sinc}(\pi \delta f t), \tag{3.4}$$

where $h(t)$ is the desired impulse response function as per Eq. (2.1) and $\text{sinc}(t) = \sin(t)/t$. This expression assumes negligibly small interpixel gaps and a focused spot size at the masking plane much less than a LCM pixel, so that the temporal window function $g(t)$ in Eq. (2.10) is much wider than the sinc function in Eq. (3.4). The result of pixelation is to produce an output pulse which is the convolution of the input pulse not only with the desired impulse response function

$h(t)$, but also with a series of replica impulse response functions, $h(t-n\delta f^{-1})$, occurring at times $t=n\delta f^{-1}$. The entire result is weighted by a temporal window function, $\mathrm{sinc}(\pi\delta f t)$, which has its first zeros at $t=\pm\delta f^{-1}$. If $h(t)$ is nonzero only during a time interval $|t|\ll\delta f^{-1}$, then the actual shaped pulse will closely approximate the desired shaped pulse, except for a few low amplitude replicas around times $t=\pm n\delta f^{-1}$. On the other hand, if $h(t)$ takes on a significant amplitude for times extending out to $|t|\sim\delta f^{-1}$, then a sort of temporal aliasing, in which the replica waveforms blend into the main waveform centered at $t=0$, will occur.

It is worth mentioning that in actual experiments, the focused spot size at the masking plane if desired can be set approximately equal to the pixel size. In this case the spectral filter function from Eq. (2.9) is a smoothed version of the spatial profile corresponding to the pixelated SLM. The corresponding Gaussian time window function significantly reduces the replica pulses predicted by Eq. (3.4). This allows the experimentalist to give up some spectral resolution (optimized by minimizing the focused spot size) for the purpose of smoothing of pixelation effects and elimination of replica pulses (by increasing the focused spot size).

Due to the effects just discussed, LC SLMs with pixel counts higher than the 128 used to date in pulse shaping would be desirable. We expect that this will be achieved in future pulse shaping instruments in view of the following considerations:

(1) LC devices with substantially higher pixel counts are in widespread use in display applications, although the specific characteristics of these LC display devices are not usually directly suitable for pulse shaping.

(2) LC SLMs with a much higher degree of sophistication than currently used for pulse shaping have been developed for beam forming and beam scanning in laser radar.[108] For example, dedicated beam steering LC SLMs with over 40 000 pixels, configured to achieve programmable linear phase sweeps (modulo 2π) via the use of up to 512 independent address lines, have been reported. These devices should be directly applicable to pulse shaping applications, since beam forming and scanning operate based on the principles of spatial Fourier optics, which are closely analogous to the principles of pulse shaping. A variety of sophisticated LCM devices are discussed in Ref. 108, which also gives an excellent overview of relevant liquid crystal principles and technology.

It is also worth noting that programmable pulse shaping using ferroelectric liquid crystals (rather than the nematic liquid crystal discussed earlier) has also been demonstrated.[109] Ferroelectric liquid crystals offer approximately two orders of magnitude faster response time ($\sim$100 μs) but are limited to binary phase modulation and generally have significant insertion loss.

B. Pulse shaping using optically addressed LC SLMs

Pulse shaping using an optically addressed LC SLM, also known as a liquid crystal light valve, was recently reported.[98] The motivation for this work is to avoid pixelation of the pulse shaping SLM.

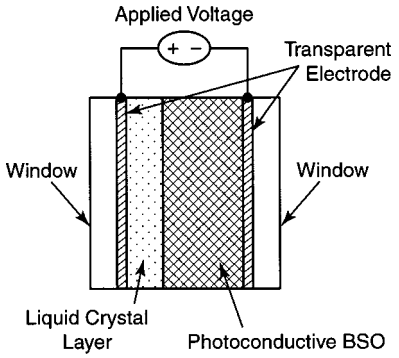

FIG. 22. Schematic diagram of an optically addressed liquid crystal light valve.

A simplified schematic of the LC light valve is shown in Fig. 22. The light valve consists of two continuous transparent electrodes and continuous layers of a twisted nematic liquid crystal and of photoconductive $Bi_{12}SiO_{20}$ (BSO). When illuminated with light in the blue green, the conductivity of the BSO layer depends on the local illumination level. When a voltage is applied between the two electrodes, a local change in the BSO conductivity results in a change in the voltage drop across the LC layer. This leads to rotation of the LC molecules and a phase change for light passing through the layer. The light valve is addressed by using a display device, such a liquid crystal television which spatially modulates light from an arc lamp. Gray-level intensity changes lead to gray-level phase shifts from the LC light valve. Pixelation effects are avoided because: (1) the light valve itself is a continuous device; and (2) the spatial frequency response of the light valve ($\sim$10 line pairs per mm) is not sufficient to resolve the small 40 μm pixels from the LC television. Therefore, the discontinuous pattern on the pixelated display device is transformed into a continuous spatial response by the LC light valve. The liquid crystal layer of the light valve is placed at the focal plane of a grating-lens pulse shaper for spectral phase filtering.

Control of the light valve is more complicated than for the electrically addressed SLMs discussed earlier, since the interaction between nearby pixels of the input display device, the limited spatial frequency response of the light valve, and the effect of illumination conditions make it difficult to compute the input image needed to achieve a specified phase pattern. To achieve a target phase pattern, an approximate (best guess) input picture was applied, and then spectral interferometry was used to measure the achieved spectral phase profile. A feedback loop then increases or decreases the local gray-level illumination intensity, depending whether the measured phase change at the corresponding wavelength is higher or lower than the target value, until convergence is achieved. Reference 98 demonstrated this method to induce arbitrary phase patterns, e.g., fourth order phase targets, with a phase control accuracy of $\sim$3%. This approach was also used to demonstrate compression of chirped pulses from a modelocked Ti:sapphire laser oscillator from 150 to 50 fs[98] and spectral phase modulation at the

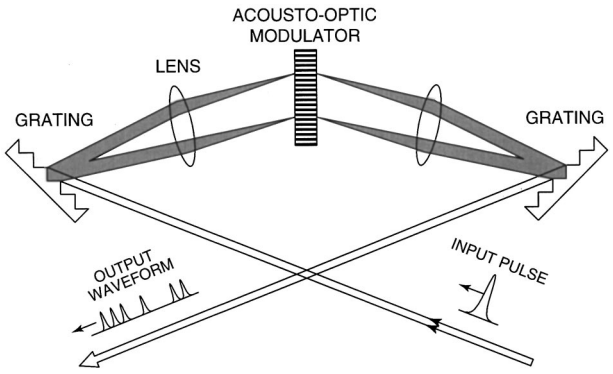

FIG. 23. Programmable pulse shaping apparatus based on the use of an AOM as the SLM.

input of a millijoule-class chirped pulse amplifier (CPA) system allowing improvement of amplified pulse quality as well as generation of antisymmetric pulse doublets at the amplifier output.[110]

In these experiments the LC light valve was able to provide a maximum phase shift of 12 rad. Unlike the pixelated LC modulators, where one can have 2π phase jumps between adjacent pixels and, hence, program desired phase functions modulo 2π, for the nonpixelated light valves abrupt phase jumps are not possible. Therefore, the total phase sweep is in fact limited to a maximum of 12 rad. Due to the limited spatial frequency response of the LC light valve, the spectral resolution of the pulse shaper was 3 nm (with the total optical bandwidth set to ~50 nm), which is significantly coarser than that obtained in experiments using pixelated LC SLMs. For these reasons, the optically addressed approach is better suited for correction of small residual phase in CPA systems than it is for generation of strongly modulated spectral phase profiles. On the other hand, liquid crystal light valves with significantly improved spatial frequency response have been reported,[111] which could potentially be applied to improve spectral resolution for pulse shaping applications.

IV. PROGRAMMABLE PULSE SHAPING USING ACOUSTO-OPTIC MODULATORS

Programmable pulse shaping based on the use of an acousto-optic modulator (AOM) as the SLM has been developed by Warren and co-workers.[80,112–114] The apparatus is depicted in Fig. 23. The AOM crystal, typically TeO_2, is driven by a radio-frequency (rf) voltage signal, which is converted into a traveling acoustic wave by a piezoelectric transducer. The acoustic wave travels across the modulator with velocity v_{ac}, leading to a refractive index grating through the photoelastic effect. The grating period Λ is given by v_{ac}/ν, where ν is the rf drive frequency. The grating can be phase, amplitude, or frequency modulated through the use of a correspondingly modulated rf drive waveform; ideally the spatial grating $s(x)$ would be related to the input voltage $v(t)$ through $s(x) \sim v(x/v_{ac})$. In practice there are a number of mechanisms which distort this ideal relationship, as discussed later. When the spatially dispersed optical frequency components diffract off the grating, the optical spectrum is modified according to the grating spatial modulation function. This results in the desired Fourier transform pulse shaping operation.

AOMs are a relatively mature technology which have been commercially available for many years. In the following we briefly describe some of the typical operating characteristics of AOMs used for pulse shaping. Further detail is given in Refs. 80 and 113.

(1) The time for the acoustic wave to move across the modulator aperture l_a is $\tau_o = l_a/v_{ac}$. This aperture time determines how quickly a new spatial pattern can be loaded into the device. For TeO_2 the acoustic velocity is $v_{ac} = 4.2\,\text{mm}/\mu\text{s}$. For the experiments reported in Refs. 112 and 80, the modulators had 5 mm and 4.3 cm apertures, respectively. The corresponding aperture times are 1.2 and 10 μs, which means that the acoustic grating pattern can be updated on a microsecond time scale.

(2) The acoustic grating pattern, which propagates across the modulator, is not fixed. Although the grating does appear frozen during readout by a single femtosecond or picosecond pulse, the pattern can shift significantly during the time between pulses for typical modelocked laser sources. For example, for a modelocked laser with 100 MHz repetition rate, the grating in a TeO_2 AOM travels by 42 μm between pulses, which is larger than the acoustic wavelength for typical drive frequencies of 100–200 MHz. Therefore, the AOM technique cannot in general be used for pulse shaping with high repetition rate laser sources, since the pulse shape would change from pulse to pulse. Note, however, that this is not a limitation for amplified ultrafast laser systems where the pulse repetition rate is usually slower than the acoustic aperture time, since this allows the acoustic pattern to be refreshed before and synchronized to each amplifier pulse. For this reason AOM pulse shaping is usually restricted to applications involving femtosecond amplifier systems.

(3) The number of independent acoustic features which can be placed within the full aperture of the AOM provides an upper limit to the pulse shaping complexity η [see Eqs. (2.12)–(2.13)], which is the same as the number of spectral features which can be placed onto the spectrum. The number of independent pixels of resolution available is proportional to $N_{\text{eff}} \sim \Delta\nu\tau_o = \Delta\nu l_a/v_{ac}$, where τ_o is the acoustic aperture time, $\Delta\nu$ is the modulation bandwidth of the AOM, and $\Delta\nu\tau_o$ is the AOM time-bandwidth product. For the large aperture ($l_a = 4.3\,\text{cm}$) AOM used in Refs. 80 and 113, the bandwidth is given as $\Delta\nu = 90\,\text{MHz}$, resulting in $\Delta\nu\tau_o \approx 900$. Therefore, an appropriate AOM should be able to place up to nearly a thousand independent features onto the spectrum, provided it is placed within an optical system with sufficient resolution. However, making use of all this potential resolution depends on setting up the pulse shaping apparatus for very high spectral resolution. To date the highest experimental resolution obtained via AOM pulse shaping appears to be on the order 100–150, which is achieved in experiments where ~75 fs input pulses are reshaped over a 10 ps window. This is comparable to what has been demonstrated in pulse shaping using LC SLMs.

(4) From an implementation perspective, it is necessary to be able to generate the complicated rf voltage waveforms

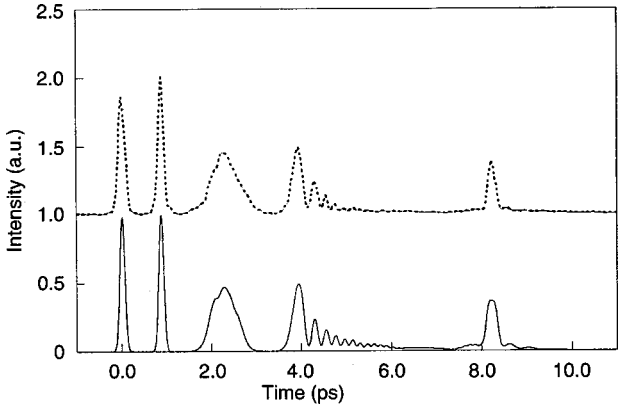

FIG. 24. Dashed line: intensity cross-correlation trace of waveform generated using an AOM in a pulse shaper. The waveform consists of an initial pulse followed by a series of delayed pulses with linear, quadratic, cubic, and quartic spectral phase, respectively. Solid line: theoretical trace.

needed to excite appropriately shaped acoustic waveforms. This can be accomplished using electronic arbitrary waveform generator (AWG) technology, which can produce complicated voltage waveforms under computer control. The most economical approach uses baseband AWGs, with bandwidths of perhaps of few tens of megahertz; the outputs from the AWGs are converted to the acousto-optic center frequency (typically a few hundred megahertz) using a simple rf oscillator and rf mixers. In these schemes two baseband AWGs may be needed, one for each quadrature of the final rf signal. An alternative but more expensive approach uses a single high-bandwidth AWG to produce the desired modulated rf waveform directly. For further discussion, see Ref. 113.

Figure 24[80] shows an example of a relatively complex experimental waveform. In this case the femtosecond pulse source was a modelocked laser oscillator with ~100 MHz repetition rate, so a boxcar integrator running at 20 kHz was used in the measurement to select those pulses for which the acoustic waveform was properly phased. The waveform consists of an initial pulse followed by a series of delayed pulses with linear, quadratic, cubic, and quartic spectral phase, respectively. Excellent agreement between experimental and theoretical cross-correlation traces was observed. A number of other complex waveforms have been reported. These include pulses with cubic spectral phase up to 90π,[113] pulses with a combined 50π cubic and 40π quintic spectral phase,[113] and amplified pulses with hyperbolic secant amplitude and hyperbolic tangent frequency sweep.[114] The latter waveform has potential applications for optical adiabatic rapid passage experiments in atomic systems.

A detailed time-frequency characterization of the frequency-swept hyperbolic secant pulse was performed[114] using the STRUT[95] technique described briefly in Sec. II G. Note that for the amplified pulse experiments, the AOM may also be programed to precompensate for residual spectral phase arising in the CPA system as well as any spectral amplitude distortion that may arise in the acousto-optic pulse shaper system.[80,114] Experimental and theoretical STRUT traces for the frequency-swept pulse, with a target analytical form given by

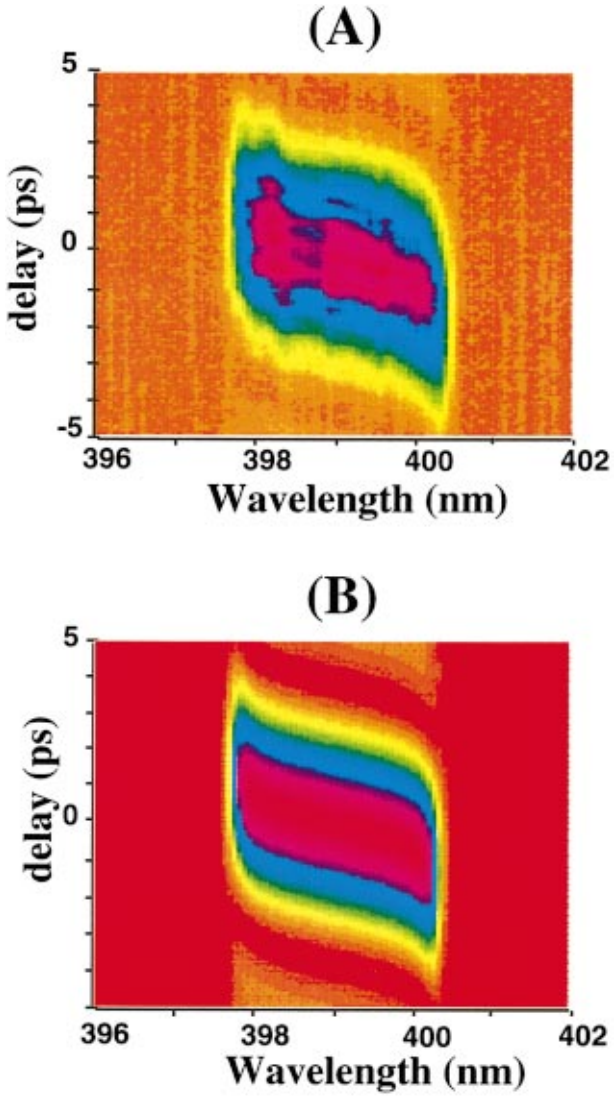

FIG. 25. (Color) (A) Experimental and (B) theoretical STRUT traces for pulse with a hyperbolic tangent frequency sweep.

$$e(t) \sim \mathrm{sech}(\rho t)^{(1+i\mu)}, \tag{4.1}$$

are shown in Fig. 25.[114] Clearly both traces show a close resemblance. For a simple interpretation of the STRUT data, recall that the measurement provides information on the frequency-dependent delay $\tau(\omega)$. The instantaneous frequency shift as a function of time can be visualized approximately by rotating the data by 90°, so that wavelength appears to plotted as a function of delay. In this orientation the data appear to take on the shape of hyperbolic tangent, which is consistent with the predicted frequency shift

$$\Delta\omega(t) = -\frac{\partial\phi(t)}{\partial t} = \rho\mu \tanh(\rho t) \tag{4.2}$$

arising from the temporal phase $\phi(t)$ in Eq. (4.1). Further data from these measurements, including the recovered spectral phase information and its derivative which gives $\tau(\omega)$ can be seen in Ref. 114.

It is useful to classify AOMs as operating in either the Raman–Nath or Bragg regime. In the Raman–Nath regime the AOM may be described as a thin grating, whereas in the Bragg regime the AOM is described as a thick (volume) grating. Quantitatively the AOM may be classified using a parameter Q, defined by

$$Q = \frac{2\pi\lambda_m L}{\Lambda^2}, \tag{4.3}$$

where L is the interaction length (thickness) in the grating, λ_m is the optical wavelength in the material, and Λ is the acoustic wavelength. The dependence of AOM operation versus Q has been discussed in the context of pulse shaping in Refs. 80 and 113. For $Q \leqslant 0.1$, the AOM is in the Raman–Nath regime, which is characterized by a diffraction efficiency which scales quadrically with acoustic amplitude and by the absence of any pronounced angular selectivity (which can lead to multiple diffracted orders from the acousto-optic grating). For $Q \geqslant 4\pi$, the AOM operates in the Bragg regime. In this regime the AOM has a strong angular selectivity, and only light incident near a certain angle (the Bragg angle) can be efficiently diffracted. The Raman–Nath regime gives the best spatial (hence, spectral) resolution due to the thin interaction region; however, the diffraction efficiency is relatively low and even in the case of very strong acoustic waves is limited to a theoretical maximum of 30% (due to diffraction into multiple orders). In the Bragg regime the diffraction efficiency can be very high (theoretically 100%), and the required acoustic amplitudes are reduced. However, the thick interaction region degrades spatial (spectral) resolution and reduces the rf as well as the optical bandwith. According to Refs. 80 and 113, a value of $Q \cong 4\pi$ appears to be a good compromise for pulse shaping applications.

There are several factors which impact the fidelity and the pulse shaping resolution available with an AOM, and predicting the detailed effect of these factors in any given situation is rather complicated. A detailed discussion is given in Refs. 80 and 113; we summarize the key points briefly later.

The pulse shaping resolution of an AOM is limited both by the minimum acoustic feature size (hence, the time-bandwidth product) and by the finite optical beam size. The beam size in turn is limited not only by the factors discussed in Sec. II C, but additionally due to the finite interaction length in an AOM operating in or near the Bragg regime. There are three principal issues, as follows:

(1) The finite interaction thickness of the AOM imposes a minimum optical spot size such that the depth of focus remains greater than or equal to the thickness. If the optical spot is further decreased, the depth of focus is also reduced, with the result that the average spot size within the interaction region actually increases! The minimum ratio of the average optical spot size to the minimum acoustic feature size can be shown to depend only on the Q parameter and the refractive index. For $Q = 4\pi$ the minimum average optical spot size is approximately equal to the minimum acoustic feature size, which means that the achievable pulse shaping resolution is somewhat reduced (by less than a factor of 2) compared to that implied by the time-bandwidth product.

(2) The input beam must be incident on the AOM at the Bragg angle $\theta_b = \lambda/2\Lambda = \lambda\nu/2v_{ac}$, were λ and Λ are the optical and acoustic wavelengths, ν is the acoustic frequency, and v_{ac} is the acoustic velocity. Since the incidence angle is therefore detuned from normal incidence, some optical frequencies will be focused before the AOM, others after the AOM. This effect becomes more important when either the acoustic center frequency (hence, the Bragg angle) or the AOM aperture is increased. A reasonable criterion is that all the optical frequencies should be focused within a Rayleigh range $\pi w_0^2/\lambda$, where w_0 is the Gaussian beam radius at the AOM. For a fixed aperture, there is a maximum acoustic frequency which satisfies this criterion. Since the modulation bandwidth of an AOM is generally proportional to the center frequency, this also limits the bandwidth and, hence, the maximum time-bandwidth product. For the 4.3 cm modulator used in Refs. 80 and 113, the maximum bandwidth is 300 MHz, which is larger than the center frequency used in the experiments.

(3) The horizontal displacement of the diffracted beam in the interaction region must be much less than the minimum acoustic feature size to avoid limiting spatial/spectral resolution. This condition is satisfied in the experiments in Refs. 80 and 113.

The pulse shaping fidelity of an AOM pulse shaper is impacted both by acoustic attenuation and acoustic nonlinearities. The intrinsic attenuation coefficient due to the material generally scales quadratically with acoustic frequency, which results in a time and frequency dependent waveform distortion (since position along the AOM aperture is proportional to time delay). Compensation for such a coupled time and frequency dependent distortion is challenging. On the other hand, at relatively low drive frequencies, other attenuation mechanisms such as acoustic walkoff related to the transducer geometry may dominate. In such cases the attenuation can be nearly frequency independent and can be calibrated simply; precompensation for the acoustic attenuation is then much easier to accomplish.

Acoustic nonlinearities can have a serious affect on pulse shaping fidelity. Acoustic nonlinearities are in general frequency, intensity, and material dependent, and are particularly strong in the TeO_2 material used in most pulse shaping experiments. Such nonlinearities can lead to intensity dependent acoustic attenuation as well as acoustic intermodulation products. In TeO_2 significant nonlinearities occur for rf powers well below those needed to reach full diffraction efficiency. Even at diffraction efficiencies of 10%–15%, there are significant nonlinear effects. Therefore, nonlinearities tend to restrict AOMs used in pulse shapers to the low diffraction efficiency regime and create complicated distortions for which precompensation is nontrivial.

One approach to improve pulse shaping fidelity without the need for a complicated theory-based precompensation procedure is to use a feedback loop in which the drive applied to the AOM is modified in response to the experimental data. This adaptive pulse shaping approach was described in Sec. II D. Adaptive pulse shaping using an AOM as the SLM has been demonstrated in quantum control experiments with amplified laser systems.[73,74] This feedback approach is espe-

cially important for AOM pulse shaping due to the waveform distortion effects discussed earlier.

The diffractive nature of the mask in AOM pulse shaping also gives rise to new dispersive effects which are not present in pulse shaping using transmissive or reflective masks or modulators. One effect is evident by referring to Fig. 23: the path lengths for optical frequency components at the top part of the figure are clearly longer than those at the bottom part of the figure.[112] Such a frequency dependent path length constitutes a dispersion, which to lowest order is a quadratic spectral phase variation. This dispersion can be compensated by changing one of the lens-grating separations or by using an external prism pair[84] compressor. Note, however, that either procedure will introduce some higher order (cubic) dispersion, which becomes more important as the pulses get shorter. A second effect involves the variation of the Bragg angle and the diffraction angle with optical frequency.[113] This effect should also become more important for shorter pulses and larger optical bandwidths. To date the shortest pulses for which AOM pulse shaping has been reported are on the order of 50 fs.[73] The effects described earlier could conceivably preclude the extension of AOM pulse shaping to shorter pulses. However, the short pulse limits of AOM pulse shaping have not yet been tested.

Although the traveling acoustic wave usually restricts AOM pulse shaping to low repetition rate experiments with amplified or pulse selected laser systems, one application for which AOM pulse shaping can be performed in conjunction with high repetition rate cw-modelocked lasers was recently reported.[115] In this application a linear phase sweep is imposed onto the spectrum, which delays the optical pulse in proportion to the amplitude of the phase sweep. This idea was previously demonstrated using a LCM array.[34,35] In the AOM case, the linear phase sweep corresponds to a simple shift in the applied rf drive frequency, which produces a pulse position modulation or tunable optical delay proportional to the rf frequency shift. Since the acoustic waveform is not spatially modulated, its motion across the aperture has no effect (except for an overall optical phase shift which varies from pulse to pulse). Experiments using 350 fs pulses in the 1.55 μm lightwave communications band achieved a tunable optical delay of 0.34 ps/MHz. Tuning was demonstrated over a delay range of 30 ps, although the pulse intensity decreased away from the center position. The delay tuning range was approximately 15 ps to maintain an intensity variation under 3 dB. The delay can be switched in only 3 μs, which is the acoustic aperture time of the AOM used in these experiments.

Reference 115 also demonstrates an interesting delay dependent dispersion effect, which would appear to apply to pulse shaping generally (not just to AOM pulse shaping). This effect arises when the diffraction gratings are not perpendicular to the optical axis of the pulse shaping system. For a tilted grating, the distance between the grating and the pulse shaping lens depends on the transverse position along the grating. As discussed in Sec. II C, a time delay in pulse shaping also corresponds to a lateral shift in the output beam[62] [see Eq. (2.14)]. This lateral shift therefore corresponds to a different lens-grating separation, which is known to give a different dispersion[42] [see Eq. (2.15)].

V. LIQUID CRYSTAL ARRAYS AND AOMs: PULSE SHAPING COMPARISON

In this section we briefly summarize Secs. III and IV by comparing LC and AOM pulse shaping technology, which are the two programmable pulse shaping approaches which have been most widely investigated. General purpose pulse shaping using deformable mirror (DM) technologies are described in Sec. VI; however, at present there is significantly less experimental experience with these devices than with LC or AOM pulse shaping. Therefore, DM pulse shaping is not included in the comparison in this section. For the LC technology, we concentrate on the nematic liquid crystal technology which has been used most extensively. We organize the discussion according to several important performance indicators, listed below. It is important to emphasize that both LC and AOM pulse shaping approaches each have their own specialized advantages, and determination of the preferred choice for a specific experiment may involve a number of trade offs depending on the most important requirements for that experiment.

(a) Pulsewidth. The LC approach has been tested down to 13 fs, and no obvious factors limiting the extension to shorter pulses have been identified. AOM shaping has been studied most extensively on the 100 fs time scale, with one experiment reporting pulses as short as 50 fs. There are several factors which are expected to make the AOM approach more difficult for much shorter pulses, although compensation of these factors may be possible. Further experiments are needed to determine the short pulse limits for both LC and AOM pulse shapers.

(b) Reprogramming time. For AOMs the reprogramming time is determined by the acoustic aperture time, which is on the order of microseconds. For nematic LC arrays, the reprogramming time is determined by the liquid crystal material response, typically on the order of 10 ms.

(c) Pulse repetition rate. Once programmed, the LCMs remain static, and therefore can handle pulse trains at virtually any repetition rate. The traveling wave nature of the AOMs generally limit these devices to pulse repetition rates slower than the acoustic aperture time. Therefore, AOMs are applicable to amplified or pulse selected systems but generally not to cw modelocked systems.

(d) Modulation format. Both LC and AOM approaches offer the ability to perform independent, gray-level spectral amplitude and phase control.

(e) Pulse shaping complexity. Pulse shaping complexity is usually defined as the number of independent features which may be placed onto the spectrum, which is equivalent to the number of independent features which may be synthesized onto the output temporal waveform [see Eq. (2.14)]. From the perspective of modulator technology, in the LC case the pulse shaping complexity is limited by the number of pixels. Current LC arrays used for pulse shaping are 128 pixel devices, although devices with larger pixel counts have been demonstrated for other applications. In the AOM case the complexity may approach the time-bandwidth product of

the modulator, which can be of order 1000 with commercially available devices. However, the pulse shaping complexity is also limited by the optical system placed around the modulator. Data representative of the highest complexity waveforms published in the literature for LC and AOM pulse shaping can be seen in Figs. 21 and 24, respectively. For Fig. 21(d), the total time window and individual pulse durations are ~4 ps and 70 fs, respectively, for a ratio of roughly 55. For Fig. 24, the corresponding numbers are ~9 ps and 90 fs, respectively, giving a ratio of roughly 100. Thus, at present the highest published complexity is somewhat less than a factor of 2 higher for AOM vs LC pulse shapers. This comparison could change in the future either due to advances in LCM technologies or due to improvements in the optical systems surrounding AOM pulse shapers.

(f) Efficiency. LCMs are inherently high efficiency devices, with transmissions approaching 100%. AOMs are typically limited to low diffraction efficiency by acoustic nonlinearities, which can be important even for diffraction efficiencies on the order of 10–15%. In both cases there are additional losses due to diffraction off the gratings, etc.

(g) Pulse shaping fidelity. Excellent pulse shaping fidelity has been achieved for both LC and AOM approaches without the need for feedback control. For the LC case, the pixelated nature of the modulator can lead to temporal sidelobes for spectral patterns which vary too rapidly from one pixel to the next. These sidelobes can be suppressed if the optical system is constructed to have a spectral resolution that results in a slight smoothing of the programed spectral pattern; however, this reduces the effective number of pixels available for pulse shaping. For the AOM case, the pulse shaping fidelity can be impacted by acoustic attenuation and acoustic nonlinearities; in general, both of these effects may be difficult to precompensate. However, under appropriate conditions very high quality waveforms with complexities on the order of 100 have been demonstrated for AOM pulse shapers, as stated earlier. For the LC and AOM data shown in Figs. 21(d) and 24, respectively, the data are in excellent agreement with the experimental target in both cases; in qualitative terms, the pulse shaping fidelity appears to be comparable for each of these data sets, at least in the estimation of this author. At present there is no standard definition of pulse shaping fidelity that can be used to characterize pulse shaping fidelity quantitatively.

(h) Technology considerations. The AOM approach uses standard AOM technology; this is a mature technology with devices available from many vendors. For the LC approach, modulator arrays have been available in appropriate formats for approximately five years from a small number of vendors (for mainstream applications such as displays, liquid crystal technology is much more highly developed). The AOM approach uses rf electronics and a single serial transducer, while 256 separate wires and a bank of low frequency electronics are used to control the 128-element amplitude and phase LC arrays.

(i) Ease of control. First we consider open loop control (the pulse shaper is not in a feedback loop). For the LC approach, the phase and amplitude response must be calibrated. However, the calibration is not too difficult and can be performed accurately enough to give very good pulse shaping results. For the AOM approach, if everything were ideal, no calibration would be necessary, at least in the low diffraction efficiency limit, where the output field is directly proportional to the acoustic complex amplitude (hence, to the voltage waveform). However, in practice a variety of factors, such as transducer impedance matching, acoustic attenuation and nonlinearities, among others, play an important role and must be taken into account. Precompensating for these effects can be nontrivial.

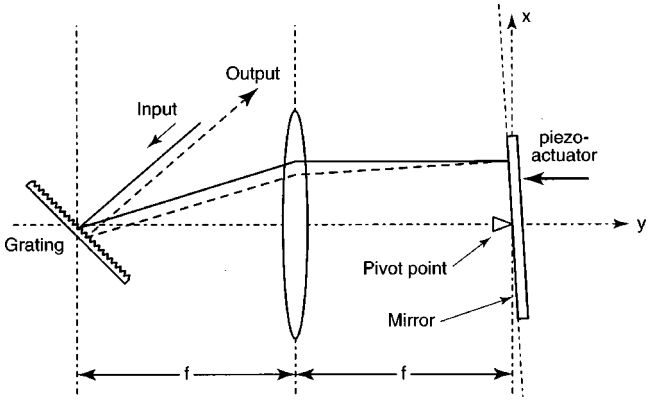

FIG. 26. Rapid scanning optical delay line based on dithering a mirror at the focal plane of a folded pulse shaper.

In the case of adaptive pulse shaping (feedback control), the control requirements are probably comparable for either pulse shaping technology, provided that target waveforms are consistent with limits imposed by the pulse shaping technology and pulse shaping physics.

VI. PULSE SHAPING USING MOVABLE AND DEFORMABLE MIRRORS

A. Moving mirrors

Several of the experimental examples discussed in previous sections involve simple forms of pure phase modulation. In particular, phase shifts which were linear, quadratic, and cubic with frequency were utilized, resulting, respectively, in pulse position modulation, chirp compensation, and a complex pulse distortion. These simple types of pure spectral phase modulation can also be produced using special purpose reflective optics, which are moved or deformed in order to assume the specific shape needed to obtain the desired phase modulation. An advantage of such special purpose movable/deformable mirrors is the ability to provide a prespecified type of phase modulation with very good precision; a disadvantage is that the arbitrary programmabiltiy available using SLMs is sacrificed.

We consider first the use of a movable mirror, which makes possible a rapid scanning optical delay line. The pulse shaping arrangement, shown in Fig. 26, consists of a grating placed in the focal plane of a lens and a planar mirror in the opposite focal plane.[116] The mirror can be dithered about the pivot point under the influence of a piezoactuator and return springs (not shown). When the tilt angle of the mirror is zero, the setup is simply a folded equivalent of a pulse shaper

without any spatial filters. When the mirror is tilted, a linear spectral phase shift is obtained, and this results in advance or retardation of the output optical pulse. The result is similar to the pulse position modulation achieved when a LC SLM or AOM is used to impart a linear phase shift onto the spectrum.

Heritage *et al.* have implemented a rapid scanning optical delay line by rapidly dithering the mirror through a small angular deflection and have used this setup to obtain femtosecond intensity correlation measurements at a 400 Hz rate.[116] This rate is much fast than possible using typical mechanical delay lines, in which the scan rate (and therefore the data acquisition rate) is limited to a few tens of hertz. For the setup described in Ref. 116, a ± 1 ps temporal delay is achieved with an angular deflection of only $\pm 1.9 \times 10^{-4}$ rad; this corresponds to a total travel of only 4 μm at the edge of the mirror. In contrast, a standard linear actuator requires a displacement of 150 μm to achieve a same 1 ps delay. This technique was later extended to provide 10 ps scans at a 2 kHz rate.[117]

Heritage *et al.* have also demonstrated a modification of this geometry which allows scanning of 90 fs pulses over a 100 ps time window.[67] The ratio of the time window to the pulse width gives a pulse shaping complexity (η) exceeding 1000, which may be the largest pulse shaping complexity yet demonstrated in Fourier transform pulse shaping. The temporal waveforms produced in these time scanning experiments are of course quite simple; they are simply shifted versions of the original pulse. By ''complexity,'' however, I have in mind the definition given in Eq. (2.14), namely the total time window divided by the shortest temporal feature, or equivalently the spectral bandwidth divided by the narrowest spectral feature. By this measure the complexity is high, since the output pulse can arrive at more than 1000 nonoverlapping temporal delays, and since in the frequency domain the linear phase sweep spans on the order of 1000π. The trick in Heritage's experiments is to retroreflect the output beam in Fig. 26 back through the reflective pulse shaper. This doubles the time delay while eliminating the spatial walkoff of the output beam. Recall that the spatial walkoff is proportional to time delay as per Eq. (2.14). With only a single pass through the pulse shaper, the time window is usually assumed to be limited to approximately that value where the spatial walkoff equals the input spot size (see Sec. II C). With double passing, this restriction is eliminated; the time window is then determined by the spatial aperture of the grating and lens, even for a relatively small input beam. A similarly large time window could also be obtained in a single pass geometry by expanding the input beam to fill the grating; however, this is usually less convenient. Note that this double-pass concept will work for pulse position modulation using any modulator technology (mirrors, LCMs, AOMs); however, it does not work for most other pulse shaping tasks.

Another useful feature is the ability to independently control the scan rates for delay and phase.[117] In contrast, when delay is varied simply by translating a mirror to change the physical path length, the phase varies by 2π for every optical cycle of delay. In the apparatus of Fig. 26, however, the phase remains fixed as the delay is scanned, provided that the mirror rotates about a pivot point at the center (or reference) optical wavelength. By translating the scanning mirror so the center wavelength is offset from the pivot point, one can select a nonzero phase scanning rate. This attribute, together with the rapid scanning delay capability, have made the moving mirror pulse shaping approach the method of choice for delay scanning in optical coherence tomography (OCT) for optical biopsies.[118] The rapid scanning is required because OCT forms an image by performing sequential rapid delay scans for a large number of independent pixels; therefore, real-time imaging requires the individual delay scans occur very quickly. The ability to independently control phase and delay scan rates allows one to select the interferometric output frequency produced by the OCT apparatus to be compatible with high performance detection and data acquisition electronics.

We briefly compare this delay scanning approach, using a moving mirror (MM) in the pulse shaper, to the case of a LC or AOM in the pulse shaper. One key difference is that the moving mirror approach is a repetitive scan technique, while the LC or AOM approaches have random access capability. The throughput of the MM approach is very high (similar to LC, higher than AOM). The speed of the MM approach is faster than for LC, and probably comparable to AOM (for the AOM approach the delay can be reset in microseconds; however many delay settings are needed to build up a full scan). The demonstrated temporal window is much higher using a MM compared to the other approaches. On the other hand, the MM approach provides only a single functionality, while LC and AOM approaches allow general purpose waveform control.

B. Deformable mirrors (DM)

In the first report of a DM in pulse shaping, the mirror was used to impart a cubic spectral phase modulation.[119] The setup is similar to that in Fig. 26, except that the MM is replaced by a DM. A cubic deflection is obtained by fixing the position of a thin planar mirror at two symmetrically placed support points and then applying equal and opposite forces on the two ends of the mirror. The desired cubic deflection is the solution of the mechanical equations governing small angle flexure of a thin elastic plate. The cubic deflection in space results in a cubic spectral phase modulation with a magnitude which can be adjusted by varying the strength of the applied forces. This third-order disperser has been applied to improve the quality of pulses from a high-power femtosecond semiconductor laser via third-order chirp compensation.[120]

Recently pulse shaping has been demonstrated using a DM phase modulator which is controlled using electrostatic rather than mechanical forces.[38] The device consists of a gold coated, silicon nitride membrane suspended over an array of electrostatic actuators. The current device has a 26 mm wide active area controlled by 13 columns of 2 mm wide actuators. The maximum deflection and the response time are reported to be 4 μm (corresponds to 20π at 800 nm wavelength) and 1 ms, respectively. Due to the relatively small

number of actuators, and the existence of a minimum radius of curvature which can be induced on the membrane, this device is mainly useful for providing smoothly varying phase variations. Experiments have been performed with a modelocked Ti:sapphire laser, where the DM pulse shaper recompressed a 15 fs pulse, which had previously been stretched to 90 fs by dispersion in glass, back to approximately the bandwidth limit,[38] and with an amplified Ti:sapphire system, where the output pulse width was improved from 20 to 15 fs.[121] The experiments also showed that longer duration stretched pulses (220 fs) were incompletely compressed due to the maximum deflection limits of the mirror.[38] Two strategies were used to control the DM. In the first the DM phase response was calibrated using FROG measurements of pulses emerging from the pulse shaper, and then desired phase functions were applied by using the previously determined calibrations. In the second the DM is used in adaptive pulse shaping mode (see Sec. II D), where a stochastic learning algorithm is used to adjust the actuator settings in order to optimize an experimental observable (e.g., second harmonic generation intensity). In the latter case precise knowledge of the DM phase response is not required. A DM pulse shaper has also be used for preliminary demonstration of a method[122] for compensating self-phase modulation in femtosecond CPAs.[123]

VII. FURTHER DIRECTIONS IN PULSE SHAPING

A. Integrated pulse shaping devices

Integration of pulse shaping devices would be desirable for applications such as optical communications where size and robustness are important. Considerable effort has been directed toward developing integrated components to handle multiple optical wavelengths for wavelength division multiplexed (WDM) optical communications networks. With suitable modification such WDM components could also be used in conjunction with femtosecond input pulses as integrated pulse shaping devices. A very simple example of pulse shaping using a device known as an integrated acousto-optic tunable filter was reported in Ref. 124. More advanced examples of pulse shaping were reported recently using modified arrayed waveguide grating routers.[125–127] There is also substantial effort in the WDM communications community to implement multichannel equalizers to correct for the wavelength dependent gain of erbium doped fiber amplifiers. Highly sophisticated arrayed waveguide grating devices have recently been demonstrated for that purpose.[128] Although these devices have not been tested with femtosecond pulses, the devices are beginning to closely resemble what would be needed for integrated pulse shaping applications.

As an alternative to integrated pulse shapers, some effort has also been directed at improving the packaging and reducing the size of bulk optics pulse shapers. For example, see Refs. 129 and 130. Several interesting examples of pulse shaping, such as generation of short pulse bursts or coded waveforms, have also been demonstrated using distributed devices such as fiber Bragg grating reflectors[131,132] and aperiodically poled second harmonic generation crystals.[133]

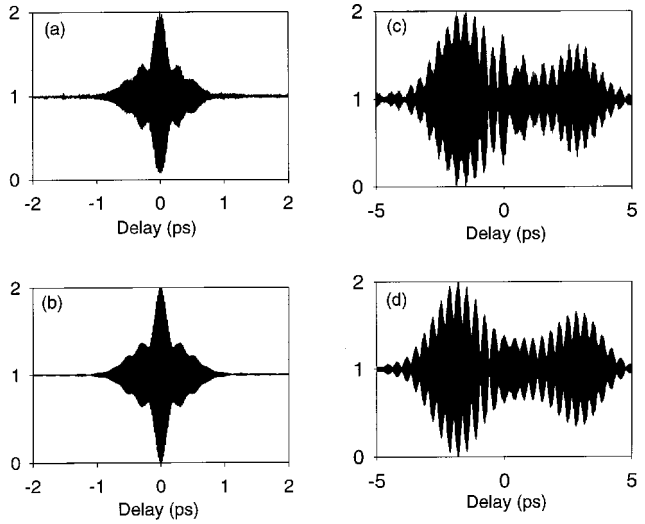

FIG. 27. Electric field cross-correlation function obtained using a pulse shaper and broadband incoherent light at 1.55 μm. (a) Experimental and (b) theoretical correlation traces of unshaped light. (c) Experimental and (d) theoretical correlation traces of shaped light using a length 31 quadratic residue spectral phase code.

However, at least till now, these distributed pulse shaping devices have not been easily reprogrammable.

B. "Pulse shaping" with incoherent light

Pulse shapers can also be used for phase filtering of broadband incoherent light. Initial experiments were performed using visible light with a few nanometers bandwidth;[134,135] subsequent experiments were performed using a programmable pulse shaper and amplified spontaneous emission from an erbium-doped fiber amplifier with several tens of nanometers bandwidth around the 1.55 μm communications band.[136] Although the result of phase filtering of incoherent light is still incoherent light, nevertheless, the phase filtering operation does affect the electric field cross-correlation function between the light before and after the pulse shaper. This can be measured by recording the interference fringes from a Michelson interferometer with a programmable pulse shaper in one arm. With this approach it has been shown that the pulse shaper can manipulate the correlation function much in the same way that a pulse shaper can manipulate the output intensity profile for coherent input pulses. An example of a shaped electric field cross-correlation function using a pulse shaper and broadband incoherent light at 1.55 μm, together with the corresponding theoretical trace, is shown in Fig. 27.[100] Motivations for performing this work include the possibility of using coherence coding of inexpensive incoherent light sources (instead of expensive femtosecond pulse sources) for certain classes of optical CDMA systems[134] and for addressing of frequency-domain optical memories.[109,135,137]

C. Pulse shaping using two-dimensional masks

Most applications of pulse shaping make use of a one-dimensional spatial mask to produce a single output beam corresponding to the desired temporal waveform. However, by using cylindrical lenses instead of spherical lenses in the

pulse shaper and by placing a two-dimensional mask at the Fourier plane, one can achieve multidimensional pulse shaping, where the output consists of a linear array of spatial beams, with each corresponding to a different independent temporal waveform. Such multidimensional pulse shaping has been demonstrated in experiments using holographic[138] as well as conventional [139] fixed two-dimensional masks, as well as in preliminary experiments using programmable two-dimensional liquid crystal arrays.[140] Using a different approach based on volume holography, formation of two-dimensional images, where each spot in the image corresponds to a different temporal waveform, has also been demonstrated.[141,142]

D. Direct space-to-time pulse shaping

The concept of a direct space-to-time (DST) pulse shaper geometry, in which the output waveform is a directly scaled version of the pulse shaping mask, has also been demonstrated. This is in contrast to the Fourier transform relationship between the mask and the temporal waveform in the conventional pulse shaping approach we have discussed in most of this article. Operation of a DST pulse shaper was first demonstrated for simple waveforms on a picosecond time scale by Emplit *et al.*[143,144] In our group we have recently demonstrated femtosecond operation of a DST pulse shaper and generation of complex optical data packets.[145] A detailed description of this pulse shaping geometry is given in Ref. 145. The main motivation for pursuing the DST shaper is for applications in high-speed information technology, such as parallel electronic to serial optical conversion and generation of ultrafast optical data packets. For these applications nanosecond to subnanosecond reprograming times are desired. This should be possible by replacing the fixed pulse shaping mask in Ref. 145 with an optoelectronic modulator array, such as a hybrid GaAs–Si complementary metal–oxide–semiconductor smart pixel array[146] or an array of asymmetric Fabry–Perot modulators.[147] Compared to the Fourier transform pulse shaper, the DST has two key advantages important for these particular applications, as follows:

(a) It avoids the need to perform a Fourier transform to determine the masking function for each new packet, which would be very difficult at high update rates, and

(b) Data packet generation using Fourier transform shaping typically requires that both spectral amplitude and phase be precisely controlled. Pulse sequence generation with a DST shaper requires only intensity modulation, which is compatible with existing optoelectronic modulator array technologies.

E. Holographic and nonlinear Fourier pulse processing and space-time conversions

Pulse shaping can be extended to accomplish more sophisticated pulse processing operations by including holographic or nonlinear materials in place of a mask or SLM within a Fourier transform pulse shaping apparatus. This results in holographic and nonlinear Fourier processing techniques which can be used for pure time-domain processing as well as time-space conversions.

We first discuss pure time-domain processing using an extension of pulse shaping called spectral holography, in which the pulse-shaping mask is replaced by a holographic material. Spectral holography was first proposed theoretically[148] in the Russian literature, and subsequent experiments demonstrating the principles of time-domain processing via spectral holography were performed by Weiner *et al.*[149,150] In analogy with off-axis spatial holography, two beams are incident: an unshaped femtosecond reference pulse with a uniform spectrum, and a temporally shaped signal waveform with information patterned onto the spectrum. The spectral components making up the reference and signal pulses are spatially dispersed and interfere at the Fourier plane. The resulting fringe pattern is stored by using a holographic medium which records a spectral hologram of the incident pulses. Readout using a short unshaped test pulse which passes through the pulse shaping apparatus results in reconstruction of real and time-reversed replicas of the original signal waveform, in analogy with the real and virtual images which are reconstructed in space-domain holography. Readout using a shaped test pulse results in output waveforms which are correlations or convolutions of the test and signal pulses. These operations, especially correlation, can be useful for matched filtering and compensation of dispersion or timing drifts. Time-domain processing using spectral holography has been demonstrated using both thermoplastic plates[149–151] (essentially a permanent recording medium) and dynamic photorefractive quantum wells (PRQWs)[152] as the holographic material.

Holographic space-to-time conversion can be achieved by placing a holographic mask at the Fourier plane of a pulse shaper. This can be achieved using either a fixed computer-generated hologram[138] or a dynamic optically addressed hologram.[97,153,154] In the case of an optically addressed hologram, the pulse shaping mask is a hologram corresponding to spatial images carried by the two input beams, which may be cw. We have recently performed space-to-time conversion experiments using PRQWs as the dynamic holographic material.[97] The temporal profile resulting when a spectrally dispersed femtosecond pulse is diffracted from the hologram can be either a direct or Fourier-transformed version of an input spatial image, depending whether a direct or Fourier transform hologram of the image is recorded. In the case of nonlinear recording conditions, additional pulse processing functions can be realized; for example, in the case of saturated holographic recording, the temporal output waveform can correspond to an edge-enhanced version of the input spatial image.[97,155] Recently, space-to-time conversion was also demonstrated by performing four-wave mixing (rather than holographic recording) at the Fourier plane of the pulse shaper, using a cascaded second order nonlinear process in a second harmonic generation crystal for the four-wave mixing interaction.[156]

Holographic and nonlinear Fourier pulse processing can also be used for time-to-space conversion of femtosecond pulses. One method for time-to-space mapping is based on recording of a spectral hologram using time-domain signal and reference pulses, as earlier, and then reading out using a monochromatic, cw laser. By passing the diffracted cw out-

put beam through a Fourier transform lens, the original temporal information is converted into spatial information. Dynamic PRQWs,[157] bulk holographic crystals,[154] and the excitonic resonance in ZnSe crystals[158] have all been employed for time-to-space conversion experiments. However, none of these materials are suitable for use in communication applications which typically require Gb/s frame rates. A related time-to-space conversion scheme relies on second harmonic generation (SHG) using a nonlinear optical crystal within a pulse shaper.[159,160] This scheme provides the fast response associated with the SHG nonlinearity, the possibility of operation at convenient wavelengths and temperatures, and the potential for high efficiency (nearly 60% harmonic conversion has been demonstrated using a modelocked oscillator source and a careful choice of nonlinear crystal).[25,161]

VIII. APPLICATIONS OF PULSE SHAPING

We conclude this review article by discussing some of the applications of femtosecond pulse shaping. Both experiments using fixed pulse shapers and programmable pulse shapers are included. Although this survey of applications is not intended to be exhaustive, nevertheless it should illustrate the breadth of areas in which pulse shaping technology is making an impact.

A. Fiber optics and photonics

1. Nonlinear optics in fibers

In ultrafast nonlinear guided wave optics, pulse shaping has been used to obtain femtosecond square pulses for all-optical switching experiments with a fiber nonlinear coupler, where square pulses gave improved switching characteristics compared to normal (unshaped) pulses by avoiding averaging over the pulse intensity profile.[45] Specially shaped and phase modulated femtosecond ''dark pulses'' were also used for the first clear demonstration of fundamental dark soliton propagation in optical fibers[78] and for subsequent dark soliton experiments performed on a picosecond time scale.[162] A brief report of an experiment where pulse shaping was used to generate phase modulated input pulses for experiments demonstrating periodic evolution and refocusing of phase modulated higher order bright solitons has also been published.[163]

2. Optical communication systems

Pulse shaping has been used extensively for studies of ultrashort pulse CDMA communications based on spectral phase encoding (see Fig. 6) and decoding, where different users share a common fiber-optic medium based on the use of different spectral codes. The CDMA receiver recognizes the desired data in the presence of multi-access interference on the basis of the strong intensity contrast between correctly and incorrectly decoded ultrashort pulses (see Fig. 28).[41] Femtosecond encoding and decoding were first demonstrated using fixed phase masks in the late 1980s,[29] and a theoretical analysis of femtosecond CDMA was reported shortly thereafter.[46] Taking advantage of advances in fiber optic technology in the early 1990s, at Purdue we have now constructed a femtosecond CDMA testbed, including encoding and decoding, dispersion compensated transmission of encoded pulses over kilometer lengths of fiber, and nonlinear optical thresholding to distinguish between correctly and incorrectly decoded pulses. Detailed discussion of our femtosecond CDMA experimental results is given in Ref. 41. Experiments on ultrashort pulse CDMA have recently been reported by industrial laboratories as well.[127,132] Pulse shaping also plays an important role in other optical CDMA schemes based on either spectral amplitude[164–166] or spectral phase[134] encoding of broadband incoherent light. Similarly spectral encoding of broadband incoherent light can be used for addressing of frequency domain optical memories based on spectral hole burning materials or volume holograms.[109,135,137] Finally, pulse shaping techniques have been extended for applications involving filtering of multiple wavelength optical signals in WDM communications. Examples include construction of WDM cross-connect switches with flat-topped frequency response[167] and multichannel WDM gain equalizers.[130]

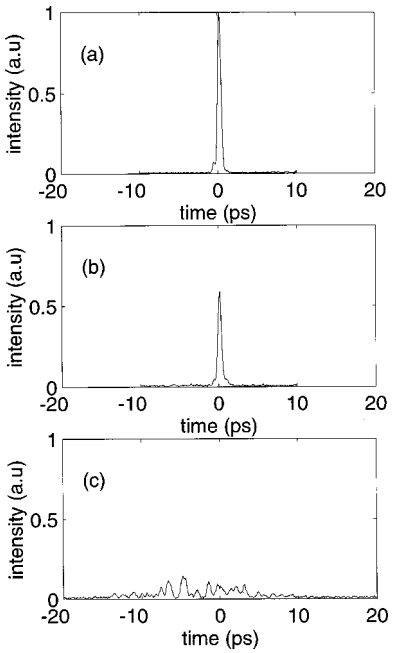

FIG. 28. Cross-correlation data obtained using ultrashort pulses at 1.55 μm and a pair of fiber-pigtailed pulse shapers. (a) Pulse which is not coded. (b) Pulse which is coded and then correctly decoded. (c) Pulse which is coded but then incorrectly decoded. Note the strong intensity contrast between correctly and incorrectly decoded pulses.

3. Novel short pulse sources

Generation of multiple streams of modelocked pulses synchronized at multiple different wavelengths has been demonstrated by introducing a pulse shaper into an external cavity modelocked semiconductor diode laser.[168] The experimental setup is sketched in Fig. 29. The grating, lens, mirror, and spatial filter combination constitute a folded pulse shaper, in which the patterned spatial filter selects which spectral components are reflected back into the gain device. Thus, the oscillating wavelengths are controlled via the selected passbands of the pulse shaper which acts as an intracavity spectral filter, while synchronization occurs via non-

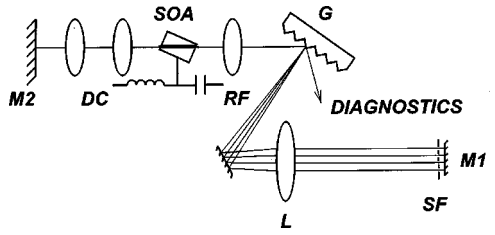

FIG. 29. Schematic layout of a multiwavelength modelocked diode laser with an intracavity pulse shaper. At 1997 IEEE.

linear interactions between different wavelengths within the diode amplifier chip. Representative wavelength tuning curves are shown in Fig. 30 for spectral filters designed to select four wavelengths. Figure 30(a) shows a four wavelength spectrum with a fixed ~1 nm spectral separation, where the center wavelength is tuned over ~18 nm in a region centered around 830 nm. Figure 30(b) shows another example where the center wavelength is held constant, while the channel spacing is tuned from 0.8 to 2.1 nm. Time-domain measurements show that the pulses on each individual wavelength channel are 12 ps in duration with a 2.5 GHz repetition frequency. Frequency-resolved optical gating measurements of these multiwavelength pulse trains have also been reported, which have been interpreted as evidence of optical phase correlations between the different oscillating wavelengths.[89] Such sources may be important in novel hybrid WDM-time-division multiplexed (TDM) communications and photonic processing schemes, and possibly can be extended to generate spectrally tailored ultrafast pulse sequences directly from modelocked lasers. In contrast to pulse shaping and spectral tailoring outside a laser, in this intracavity pulse shaping work all the available energy is preserved but caused to appear at the selected wavelengths.

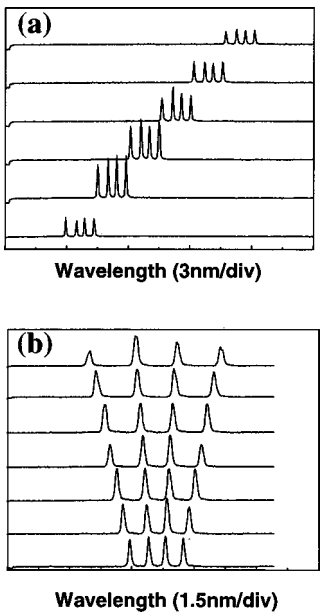

FIG. 30. Wavelength tuning curves for modelocked diode laser with intracavity pulse shaper. (a) Tuning over 18 nm with wavelength separation held constant. (b) Control of the wavelength channel spacing. At 1997 IEEE.

4. Dispersion compensation

Dispersion compensation for fiber communications was discussed in Sec. III A. Briefly, a programmable pulse shaper was used as a spectral phase equalizer in conjunction with dispersion compensated fiber links, resulting in distortion-free transmission of 400 fs pulses over 10 km of fiber.[40,103] This approach may be important for ultrashort pulse CDMA and several hundred Gb/s TDM communications, both of which are sensitive to higher order phase dispersion.

5. Space-time conversions

Space-time conversions, outlined briefly in Secs. VII D and VII E, may be important for generation, demultiplexing, and processing of very high rate optical data sequences. Space-time conversion and its applications are discussed further in Refs. 25, 145, and 169.

B. Biomedical applications

We have already mentioned (Sec. VI A) that a pulse shaping approach, based on a moving mirror at the Fourier plane, has become the method of choice for rapid time delay scanning in OCT biomedical imaging.[117,118] Pulse shaping is also being investigated for applications in multiphoton confocal microscopy.[170] Here the goal is to tailor the pulse shape to maximize the efficiency of the nonlinear process, which is important in order to generate a bright image while minimizing the exposure of sensitive biological samples to laser radiation.

C. Phase control in femtosecond amplifiers

Precise and complete chirp compensation is one of the key issues in optimizing pulse quality in femtosecond CPA systems.[22,43] Spectral phase control is important both in obtaining the minimum pulse width and in suppressing wings and sidelobes in the compressed pulse, since pulses with extremely high on-off contrast are needed for most high intensity applications. Pulse shaping is increasingly being considered for such phase control. In one early example, third and fourth order spectral phase were both compensated by adjusting a custom air-spaced doublet lens placed with a pulse shaper,[171] resulting in dramatically decreased temporal wings. More recently, a number of groups are using programmable pulse shapers for such spectral phase compensation in femtosecond amplifiers.[69,71,114,121] Results have been published for several different programmable pulse shaping technologies, and experiments on amplified pulses as short as ~15 fs have been reported.[121]

It should be noted that phase compensation of CPA systems is possible down to at least the sub-30- fs regime without the use of programmable techniques such as pulse shaping,[22] although this requires considerable care. Pulse shaping is being applied for two reasons. The first is to achieve phase compensation, and hence, shorter, higher quality pulses, at durations beyond the experimental state of the art. The second is simply to be able to use a CPA system which has been constructed without completely optimizing the spectral phase, and still be able to make it perform at near

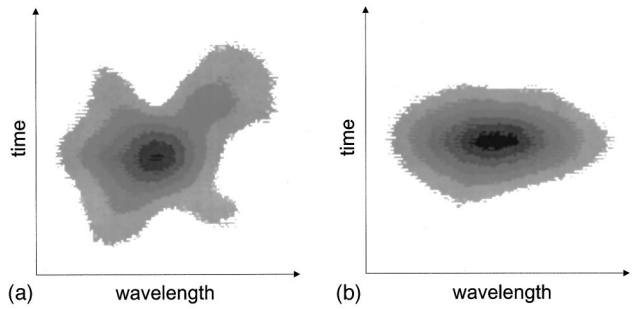

FIG. 31. (a) FROG trace of original, phase distorted amplified pulses. (b) FROG trace of optimized pulse after phase correction by programmable pulse shaper.

the bandwidth limit. In the latter case, the advantage is that it gives the experimentalist more options for accomplishing the phase correction.

Data from an experiment where a pulse shaper with a phase-only LCM is placed after a CPA are plotted in Figs. 31 and 32.[71] The pulses are centered at 800 nm with a bandwidth of ~8 nm, and the pulse energy after the pulse shaper is 200 μJ at a 1 kHz repetition rate. The duration of the amplified pulses without correction by the pulse shaper was 195 fs, roughly a factor of 2 above the bandwidth limit. By using the pulse shaper for phase correction, which was adjusted via adaptive feedback under control of an evolutionary algorithm, the pulses were compressed to 103 fs, close to the bandwidth limit. FROG traces of the pulses based on SHG gating[87] with and without phase correction are shown in Figs. 31(a) and 31(b), respectively. For interpreting these traces, the main point is that a bandwidth-limited pulse is expected to have a simple elliptical SHG–FROG trace, with major and minor axes pointing along the wavelength and time axes. A simple linear chirp leads to an increase in the area of this ellipse, without changing its orientation. More complex structure is indicative of higher-order phase variations. Thus, the irregular uncorrected FROG trace in Fig. 31(a) shows signs of a complex spectral phase, which appears to be almost completely eliminated in the phase-corrected plot. This is also evident in the time domain intensity and phase profiles (Fig. 32) retrieved from the FROG data. The intensity profile is significantly smoother and shorter after phase correction, and the temporal phase profile after the correction is almost flat in the region where there is significant intensity.

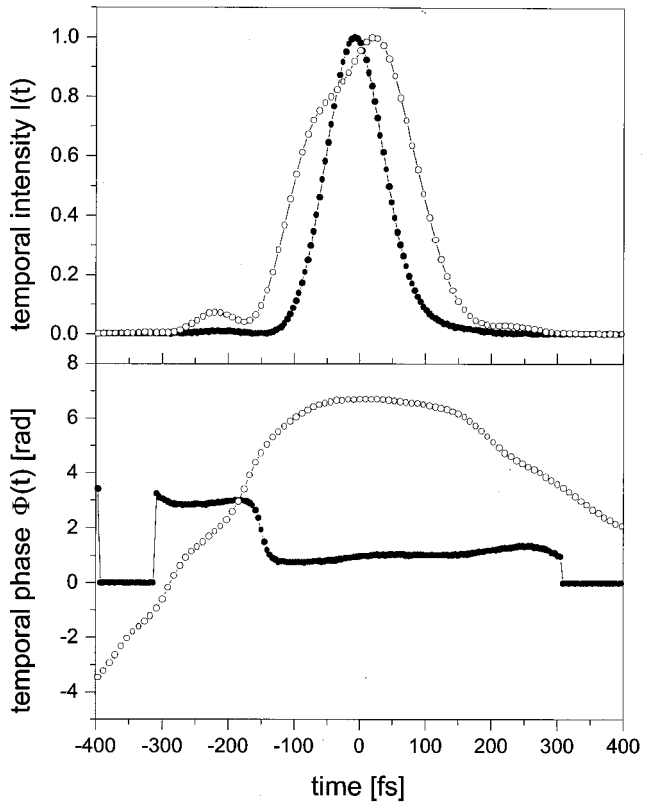

FIG. 32. Retrieved time-domain intensity (upper plot) and phase (lower plot) profiles of amplified pulses for original (open circles) and phase-corrected (full circles) amplified pulses.

D. Bandpass filtering

A very simple application uses a pulse shaper with an adjustable slit at the Fourier plane to implement a variable bandpass optical filter. This technique has been used by several groups to generate tunable, bandwidth limited pulses from a femtosecond white-light continuum, which have been applied, for example, for time-resolved spectroscopy of semiconductors[172,173] and nanocrystals[174] and high intensity studies of atomic gases.[175] In some experiments a pair of pulse shapers is used to carve synchronized pulses from a white-light continuum at different independently tunable wavelengths.[173] Such bandpass filtering can also be used in conjunction with coherent modelocked lasers, leading to pulsewidth control in the time domain, which was used for example to measure the pulsewidth dependence of two photon absorption in nonlinear waveguide photodetectors[176] and for studies of polariton scattering in semiconductor microcavities.[177]

E. Control of quantum dynamics and nonlinear optics

Pulse shaping plays a major role in the field of coherent or quantum control, in which the experimentalist seeks to manipulate quantum mechanical wave packets via the phase and intensity profiles of the exciting laser radiation. Since many of the quantum mechanical motions of interest occur on an ultrafast time scale, femtosecond pulse shaping is often needed to create the required laser profiles. For a review of the quantum control field, see Ref. 75.

In one of the earliest femtosecond coherent control experiments, terahertz rate trains of femtosecond pulses were used to achieve selective amplification of optical phonons via multiple pulse impulsive stimulated Raman scattering (ISRS).[50,51,178] The input pulse trains were generated by phase-only filtering in a pulse shaper.[47] These ISRS experiments were sensitive only to the optical intensity profile (hence, the pulse timing) but not to optical phase. Related experiments were later extended for phase-sensitive manipulation of coherent charge oscillations in semiconductor multiple quantum wells.[52,53]

Another simple example involves multidimensional spectroscopic studies using two and three pulse sequences with specified phase relationships and interpulse delays to excite specified coherent states in an atomic vapor.[105] This leads to control of the fluorescent yield as a function of the delays and phases, which were varied using a dual LCM array in the pulse shaper. The variations in the fluorescence yield may be understood as arising from different degrees of overlap of the optical power spectrum, which is relatively highly structured and which depends on the pulse timings and phases, with the atomic absorption spectrum. A review of the application of such pulse sequences to multidimensional spectroscopy and optical control is given in Ref. 105. Note that similar experiments using two-pulse sequences can be performed conveniently by using a stabilized interferometer to generate the phase-locked pulse pairs.[179,180] Phase-locked three pulse sequences are more complex to generate via interferometers; at this level of complexity, pulse shaping is the best choice.

More generally, one often desires more complicated ultrafast waveforms to generate wave packets and wave functions that could not be obtained otherwise. In the weak field case, Wilson's group for example calculated ''globally optimum weak light fields'' giving the best possible overlap with specified molecular dynamics outcomes.[181–183] Cases studied include a ''molecular cannon,'' in which an outgoing continuum wave packet in I_2 is focused in both space and momentum, and a ''reflectron,'' resulting in focusing of an incoming bound wave packet in I_2, among others. In the strong field regime, theory suggests a number of exciting possibilities for coherent control through shaped pulses or pulse sequences, including breaking strong bonds and manipulating reaction pathways and curve crossings,[184–188] to name just a few.

Experiments are beginning to yield interesting results. Pulse shaping has been used in a series of experiments in Rydberg atoms, for example, where custom Rydberg wave packets have been produced as well as measured.[74] Control of fluorescent yields in dye molecules[73] and optimization of branching ratios of different photodisassociation reaction channels of organometallic molecules has also been reported.[72] Many of these experiments were performed in an adaptive pulse shaping configuration (see Sec. II D). Other works were performed using open-loop pulse shaping. These include a series of studies on coherent control of spin and population dynamics in quantum wells[189] and experiments on coherent control of resonant two photon absorption in atomic argon as a function of the optical phase modulation.[190]

Pulse shaping can also be used for control of nonlinear optical processes which are not inherently quantum mechanical. For example, in SHG, spectral amplitude masking of chirped pulses was used to achieve both good efficiency and a narrow second harmonic bandwidth simultaneously, despite the broad bandwidth of the excitation pulses.[191,192] This focusing of spectral energy was related to focusing in free space by a Fresnal zone plate. Similar experiments were also performed for two photon absorption[191,192] In a second example related to terahertz (THz) radiation, shaped optical pulse sequences were used to excite photoconductive antennas, resulting in the ability to manipulate the emitted THz radiation waveform.[193] This technique has also resulted in enhancements of the emitted peak THz power spectral density due to avoidance of saturation mechanisms through multiple pulse excitation.[54,194]

F. Laser-electron beam interactions

Several schemes have been proposed in which pulse shaping would favorably enhance laser-electron interactions. One application involves laser generation of large amplitude, relativistic plasma waves (with application to ultrahigh-gradient electron accelerators). It has been shown theoretically that by using an appropriate femtosecond pulse sequence, one could in principle drive plasma oscillations to larger amplitudes than possible with a single pulse of the same total energy.[195,196] By using a pulse sequence, one could compensate for the change is plasma frequency arising when the plasma enters the large amplitude, nonlinear regime, in addition to avoiding various laser-plasma instabilities through the use of lower peak intensities. The use of pulse shaping to seed other desirable plasma instabilities has also been proposed.[197] Further possibilities, such as using pulse shaping (a) to generate energetically and temporally modulated electron beams to enhance the generation of short wavelength radiation in free electron lasers[198] or (b) to modify the spectra produced under the influence of nonlinear Doppler shifts in relativistic Compton backscattering,[199] have also been discussed.

ACKNOWLEDGMENTS

This work was supported in part by the Army Research Office under DAAG55-98-1-0514 and by the National Science Foundation under 9626967-ECS and 9722668-PHY.

[1] R. L. Fork, B. I. Greene, and C. V. Shank, Appl. Phys. Lett. **38**, 671 (1981).
[2] C. V. Shank, R. L. Fork, R. Yen, R. H. Stolen, and W. J. Tomlinson, Appl. Phys. Lett. **40**, 761 (1982).
[3] J. G. Fujimoto, A. M. Weiner, and E. P. Ippen, Appl. Phys. Lett. **44**, 832 (1984).
[4] J.-M. Halbout and D. Grischkowsky, Appl. Phys. Lett. **45**, 1281 (1984).
[5] W. H. Knox, R. L. Fork, M. C. Downer, R. H. Stolen, C. V. Shank, and J. A. Valdmanis, Appl. Phys. Lett. **46**, 1120 (1985).
[6] R. L. Fork, C. H. Brito Cruz, P. C. Becker, and C. V. Shank, Opt. Lett. **12**, 483 (1987).
[7] D. E. Spence, P. N. Kean, and W. Sibbett, Opt. Lett. **16**, 42 (1991).
[8] M. T. Asaki, C.-P. Huang, D. Garvey, J. Zhou, H. C. Kapteyn, and M. M. Murnane, Opt. Lett. **18**, 977 (1993).
[9] J. Zhou, G. Taft, C.-P. Huang, M. M. Murnane, and H. C. Kapteyn, Opt. Lett. **19**, 1149 (1994).
[10] A. Stingl, M. Lenzner, Ch. Spielmann, F. Krausz, and R. Szipocs, Opt. Lett. **20**, 602 (1995).
[11] I. Jung *et al.*, Opt. Lett. **22**, 1009 (1998).
[12] L. Xu, G. Tempea, Ch. Spielmann, F. Krausz, A. Stingl, K. Ferencz, and S. Takano, Opt. Lett. **23**, 789 (1998).
[13] U. Morgner *et al.*, Opt. Lett. **24**, 411 (1999).
[14] D. H. Sutter *et al.*, Opt. Lett. **24**, 631 (1999).
[15] M. Nakazawa, ed., IEICE Trans. **E81–C**, 93 (1998).
[16] U. Keller, ed., Appl. Phys. B: Lasers Opt. **65**, 113 (1997).
[17] C. P. J. Barty, W. White, W. Sibbett, and R. Trebino, eds., IEEE J. Sel. Top. Quantum Electron. **4**, 157 (1998).
[18] W. Kaiser, *Ultrashort Laser Pulses and Applications* (Springer, Berlin, 1988).

[19] J. C. Diels and W. Rudolph, *Ultrahort Laser Pulse Phenomena* (Academic, San Diego, 1996).
[20] *Ultrafast Phenomena XI*, edited by T. Elsaesser, J. G. Fujimoto, D. A. Wiersma, and W. Zinth (Springer, Berlin, Germany, 1998).
[21] C. Rulliere, *Femtosecond Laser Pulses* (Springer, Berlin, 1998).
[22] S. Backus, C. G. Durfee III, M. M. Murnane, and H. C. Kapteyn, Rev. Sci. Instrum. **69**, 1207 (1998).
[23] C. Froehly, B. Colombeau, and M. Vampouille, in *Progress in Optics*, edited by E. Wolf (North-Holland, Amsterdam, 1983), Vol. 20, pp. 65–153.
[24] A. M. Weiner and J. P. Heritage, Rev. Phys. Appl. **22**, 1619 (1987).
[25] A. M. Weiner and A. M. Kanan, IEEE J. Sel. Top. Quantum Electron. **4**, 317 (1998).
[26] A. M. Weiner, in *Trends in Optics and Photonics*, edited by T. Asakura (Springer, Berlin, 1999), pp. 233–246.
[27] A. M. Weiner, Prog. Quantum Electron. **19**, 161 (1995).
[28] A. M. Weiner, J. P. Heritage, and E. M. Kirschner, J. Opt. Soc. Am. B **5**, 1563 (1988).
[29] A. M. Weiner, J. P. Heritage, and J. A. Salehi, Opt. Lett. **13**, 300 (1988).
[30] D. H. Reitze, A. M. Weiner, and D. E. Leaird, Appl. Phys. Lett. **61**, 1260 (1992).
[31] J. P. Heritage, R. N. Thurston, W. J. Tomlinson, A. M. Weiner, and R. H. Stolen, Appl. Phys. Lett. **47**, 87 (1985).
[32] J. P. Heritage, A. M. Weiner, and R. N. Thurston, Opt. Lett. **10**, 609 (1985).
[33] A. M. Weiner, J. P. Heritage, and R. N. Thurston, Opt. Lett. **11**, 153 (1986).
[34] A. M. Weiner, D. E. Leaird, J. S. Patel, and J. R. Wullert, Opt. Lett. **15**, 326 (1990).
[35] A. M. Weiner, D. E. Leaird, J. S. Patel, and J. R. Wullert, IEEE J. Quantum Electron. **28**, 908 (1992).
[36] A. Efimov, C. Schaffer, and D. H. Reitze, J. Opt. Soc. Am. B **12**, 1968 (1995).
[37] D. Yelin, D. Meshulach, and Y. Silberberg, Opt. Lett. **22**, 1793 (1997).
[38] E. Zeek, K. Maginnis, S. Backus, U. Russek, M. Murnane, G. Mourou, H. Kapteyn, and G. Vdovin, Opt. Lett. **24**, 493 (1999).
[39] C.-C. Chang, H. P. Sardesai, and A. M. Weiner, IEEE Photonics Technol. Lett. **10**, 171 (1998).
[40] C.-C. Chang, H. P. Sardesai, and A. M. Weiner, Opt. Lett. **23**, 283 (1998).
[41] H. P. Sardesai, C.-C. Chang, and A. M. Weiner, J. Lightwave Technol. **16**, 1953 (1998).
[42] O. E. Martinez, IEEE J. Quantum Electron. **23**, 59 (1987).
[43] P. Maine, D. Strickland, P. Bado, M. Pessot, and G. Mourou, IEEE J. Quantum Electron. **24**, 398 (1988).
[44] K. C. Chu, J. P. Heritage, R. S. Grant, and W. E. White, Opt. Lett. **21**, 1842 (1996).
[45] A. M. Weiner, Y. Silberberg, H. Fouckhardt, D. E. Leaird, M. A. Saifi, M. J. Andrejco, and P. W. Smith, IEEE J. Quantum Electron. **25**, 2648 (1989).
[46] J. A. Salehi, A. M. Weiner, and J. P. Heritage, J. Lightwave Technol. **8**, 478 (1990).
[47] A. M. Weiner and D. E. Leaird, Opt. Lett. **15**, 51 (1990).
[48] A. M. Weiner, S. Oudin, D. E. Leaird, and D. H. Reitze, J. Opt. Soc. Am. A **10**, 1112 (1993).
[49] R. Skaug and J. F. Hjelmstad, *Spread Spectrum in Communications* (Peregrinus, London, 1985).
[50] A. M. Weiner, D. E. Leaird, G. P. Wiederrecht, and K. A. Nelson, Science **247**, 1317 (1990).
[51] A. M. Weiner, D. E. Leaird, G. P. Wiederrecht, and K. A. Nelson, J. Opt. Soc. Am. B **8**, 1264 (1991).
[52] I. Brener, P. C. M. Planken, M. C. Nuss, L. Pfeiffer, D. E. Leaird, and A. M. Weiner, Appl. Phys. Lett. **63**, 2213 (1993).
[53] I. Brener, P. C. M. Planken, M. C. Nuss, M. S. C. Luo, S. L. Chuang, L. Pfeiffer, D. E. Leaird, and A. M. Weiner, J. Opt. Soc. Am. B **11**, 2457 (1994).
[54] Y. Liu, S.-G. Park, and A. M. Weiner, Opt. Lett. **21**, 1762 (1996).
[55] H. Dammann and K. Gortler, Opt. Commun. **3**, 312 (1971).
[56] H. Dammann and E. Klotz, Opt. Acta **24**, 505 (1977).
[57] U. Killat, G. Rabe, and W. Rave, Fiber Integr. Opt. **4**, 159 (1982).
[58] M. C. Wefers and K. A. Nelson, Opt. Lett. **18**, 2032 (1993).
[59] K. Takasago, M. Takekawa, F. Kannari, M. Tani, and K. Sakai, Jpn. J. Appl. Phys., Part 2 **35**, L1430 (1996).
[60] K. Takasago, M. Takekawa, M. Suzuki, K. Komori, and F. Kannari, IEEE J. Sel. Top. Quantum Electron. **4**, 346 (1998).
[61] M. B. Danailov and I. P. Christov, J. Mod. Opt. **36**, 725 (1989).
[62] M. M. Wefers and K. A. Nelson, IEEE J. Quantum Electron. **32**, 161 (1996).
[63] J. Paye and A. Migus, J. Opt. Soc. Am. B **12**, 1480 (1995).
[64] R. N. Thurston, J. P. Heritage, A. M. Weiner, and W. J. Tomlinson, IEEE J. Quantum Electron. **22**, 682 (1986).
[65] C. Dorrer and F. Salin, IEEE J. Sel. Top. Quantum Electron. **4**, 342 (1998).
[66] I. Lorgere, M. Ratsep, J.-L. Le Gouet, F. Grelet, M. Tian, A. Debarre, and P. Tchenio, J. Phys. B **28**, L565 (1995).
[67] K. C. Chu, K. Liu, J. P. Heritage, and A. Dienes, presented at the Conference on Lasers and Electro-optics, Anaheim, CA, 1994.
[68] D. Meshulach, D. Yelin, and Y. Silberberg, J. Opt. Soc. Am. B **15**, 1615 (1998).
[69] A. Efimov, M. D. Moores, N. M Beach, J. L. Krause, and D. H. Reitze, Opt. Lett. **23**, 1915 (1998).
[70] T. Baumert, T. Brixner, V. Seyfried, M. Strehle, and G. Gerber, Appl. Phys. B: Lasers Opt. **65**, 779 (1997).
[71] T. Brixner, M. Strehle, and G. Gerber, Appl. Phys. B: Lasers Opt. **68**, 281 (1999).
[72] A. Assion, T. Baumert, M. Bergt, T. Brixner, B. Kiefer, V. Seyfried, M. Strehle, and G. Gerber, Science **282**, 919 (1998).
[73] C. J. Bardeen, V. V. Yakovlev, K. R. Wilson, S. D. Carpenter, P. M. Weber, and W. S. Warren, Chem. Phys. Lett. **280**, 151 (1997).
[74] T. C. Weinacht, J. Ahn, and P. H. Bucksbaum, Nature (London) **397**, 233 (1999).
[75] W. S. Warren, R. Rabitz, and M. Dahleh, Science **259**, 1581 (1993).
[76] R. S. Judson and H. Rabitz, Phys. Rev. Lett. **68**, 1500 (1992).
[77] Y. J. Yan, B. E. Kohler, R. E. Gillilan, R. M. Whitnell, K. R. Wilson, and S. Mukamel, in *Ultrafast Phenomena VIII*, edited by J.-L. Martin, A. Migus, G. A. Mourou, and A. H. Zewail (Springer, Berlin, 1992), pp. 8–12.
[78] A. M. Weiner, J. P. Heritage, R. J. Hawkins, R. N. Thurston, E. M. Kirschner, D. E. Leaird, and W. J. Tomlinson, Phys. Rev. Lett. **61**, 2445 (1988).
[79] A. M. Weiner, R. N. Thurston, W. J. Tomlinson, J. P. Heritage, D. E. Leaird, E. M. Kirschner, and R. J. Hawkins, Opt. Lett. **14**, 868 (1989).
[80] M. A. Dugan, J. X. Tull, and W. S. Warren, J. Opt. Soc. Am. B **14**, 2348 (1997).
[81] X. Liu, R. Wagner, A. Maksimchuk, E. Goodman, J. Workman, D. Umstadter, and A. Migus, Opt. Lett. **20**, 1163 (1995).
[82] A. Efimov and D. H. Reitze, Opt. Lett. **23**, 1612 (1998).
[83] A. E. Treacy, IEEE J. Quantum Electron. **5**, 454 (1969).
[84] O. E. Martinez, J. P. Gordon, and R. L. Fork, J. Opt. Soc. Am. A **1**, 1003 (1984).
[85] E. P. Ippen and C. V. Shank, in *Ultrashort Light Pulses*, edited by S. L. Shapiro (Springer, Berlin, 1977), pp. 85–88.
[86] R. Trebino and D. J. Kane, J. Opt. Soc. Am. A **10**, 1101 (1993).
[87] R. Trebino, K. W. DeLong, D. N. Fittinghoff, J. N. Sweetser, M. A. Krumbugel, and B. A. Richman, Rev. Sci. Instrum. **68**, 3277 (1997).
[88] B. Kohler, V. V. Yakovlev, K. R. Wilson, J. Squier, K. W. DeLong, and R. Trebino, Opt. Lett. **20**, 483 (1995).
[89] H. Shi, I. Nitta, A. Schober, P. J. Delfyett, G. Alphonse, and J. Connolly, Opt. Lett. **24**, 238 (1999).
[90] F. G. Omenetto, J. W. Nicholson, and A. J. Taylor, Opt. Lett. **24**, 1780 (1999).
[91] J. L. A. Chilla and O. E. Martinez, Opt. Lett. **16**, 39 (1991).
[92] J. L. A. Chilla and O. E. Martinez, IEEE J. Quantum Electron. **27**, 1228 (1991).
[93] J.-P. Foing, J.-P. Likorfman, M. Joffre, and A. Migus, IEEE J. Quantum Electron. **28**, 2285 (1992).
[94] J.-K. Rhee, T. S. Sosnowski, T. B. Norris, J. A. Arns, and W. S. Coburn, Opt. Lett. **19**, 1550 (1994).
[95] J.-K. Rhee, T. S. Sosnowski, A.-C. Tien, and T. B. Norris, J. Opt. Soc. Am. B **13**, 1780 (1996).
[96] L. Lepetit, G. Cheriaux, and M. Joffre, J. Opt. Soc. Am. B **12**, 2467 (1995).
[97] Y. Ding, D. D. Nolte, M. R. Melloch, and A. M. Weiner, IEEE J. Sel. Top. Quantum Electron. **4**, 332 (1998).
[98] C. Dorrer, F. Salin, F. Verluise, and J. P. Huignard, Opt. Lett. **23**, 709 (1998).
[99] C. Dorrer and F. Salin, J. Opt. Soc. Am. B **15**, 2331 (1998).

[100] L. Wang and A. M. Weiner, Opt. Commun. **167**, 211 (1999).
[101] C.-C. Chang and A. M. Weiner, IEEE J. Quantum Electron. **33**, 1455 (1997).
[102] P. G. deGennes, *The Physics of Liquid Crystals* (Clarendon, Oxford, 1974).
[103] S. Shen and A. M. Weiner, IEEE Photonics Technol. Lett. **11**, 827 (1999).
[104] M. M. Wefers and K. A. Nelson, Opt. Lett. **20**, 1047 (1995).
[105] H. Kawashima, M. M. Wefers, and K. A. Nelson, Annu. Rev. Phys. Chem. **46**, 627 (1995).
[106] S. Shen and A. M. Weiner, IEEE Photonics Technol. Lett. **11**, 566 (1999).
[107] Z. Zheng (personal communication).
[108] P. F. McManamon *et al.*, Proc. IEEE **84**, 268 (1996).
[109] M. Ratsep, M. Tian, I. Lorgere, F. Grelet, and J.-L. Le Gouet, Opt. Lett. **21**, 83 (1996).
[110] C. Dorrer, C. Le Blanc, and F. Salin, presented at the CLEO Europe, Glasgow, Scotland, 1998.
[111] Y. Igasaki, N. Yoshida, H. Toyoda, Y. Kobayashi, N. Mukohzaka, and T. Hara, Opt. Rev. **4**, 167 (1997).
[112] C. W. Hillegas, J. X. Tull, D. Goswami, D. Strickland, and W. S. Warren, Opt. Lett. **19**, 737 (1994).
[113] J. X. Tull, M. A. Dugan, and W. S. Warren, Adv. Magn. Opt. Reson. **20**, 1 (1997).
[114] M. R. Fetterman, D. Goswami, D. Keusters, W. Yang, J.-K. Rhee, and W. S. Warren, Opt. Express **3**, 366 (1998).
[115] W. Yang, D. Keusters, D. Goswami, and W. S. Warren, Opt. Lett. **23**, 1843 (1998).
[116] K. F. Kwong, D. Yankelevich, K. C. Chu, J. P. Heritage, and A. Dienes, Opt. Lett. **18**, 558 (1993).
[117] G. J. Tearney, B. E. Bouma, and J. G. Fujimoto, Opt. Lett. **22**, 1811 (1997).
[118] G. J. Tearney, M. E. Brezinski, B. E. Bouma, S. A. Boppart, C. Pitris, J. F. Southern, and J. G. Fujimoto, Science **276**, 2037 (1997).
[119] J. P. Heritage, E. W. Chase, R. N. Thurston, and M. Stern, presented at the Conference on Lasers and Electro-optics, Baltimore, MD, 1991.
[120] P. J. Delfyett, L. T. Florez, N. Stoffel, T. Gmitter, N. C. Andreadakis, Y. Silberberg, J. Heritage, and G. Alphonse, IEEE J. Quantum Electron. **28**, 2203 (1992).
[121] E. Zeek, S. Backus, R. Bartles, H. Kapteyn, and M. Murnane, presented at the Conference on Lasers and Electro-optics, Baltimore, MD, 1999.
[122] A. Braun, S. Kane, and T. Norris, Opt. Lett. **22**, 615 (1997).
[123] L. R. Bruner, O. Albert, G. Cheriaux, G. Mourou, T. Norris, and G. Vdovin, presented at the Conference on Lasers and Electro-optics, Baltimore, MD, 1999.
[124] M. E. Fermann, V. Da Silva, D. A. Smith, Y. Silberberg, and A. M. Weiner, Opt. Lett. **18**, 1505 (1993).
[125] T. Kurokawa, H. Tsuda, K. Okamoto, K. Naganuma, H. Takenouchi, Y. Inoue, and M. Ishii, Electron. Lett. **33**, 1890 (1997).
[126] H. Takenouchi, H. Tsuda, K. Naganuma, T. Kurokawa, Y. Inoue, and K. Okamoto, Electron. Lett. **34**, 1245 (1998).
[127] H. Tsuda, H. Takenouchi, T. Ishii, K. Okamoto, T. Gosh, and C. Amano, presented at the Optical Fiber Communications, San Diego, CA, 1999.
[128] C. R. Doerr, P. Schiffer, L. W. Stulz, M. Cappuzzo, E. Laskowski, A. Paunescu, L. Gomez, and J. Gates, presented at the Optical Fiber Communications, San Diego, CA, 1999.
[129] R. Grote and H. Fouckhardt, presented at the Optical Fiber Communications, San Diego, CA, 1999.
[130] J. E. Ford and J. A. Walker, IEEE Photonics Technol. Lett. **10**, 1440 (1998).
[131] L. R. Chen, S. D. Benjamin, P. W. E. Smith, J. E. Sipe, and S. Juma, Opt. Lett. **22**, 402 (1997).
[132] A. Grunnet-Jepsen, A. Johnson, E. Maniloff, T. W. Mossberg, M. J. Munroe, and J. N. Sweetser, presented at the Optical Fiber Communications, San Diego, CA, 1999.
[133] G. Imeshev, A. Galvanauskas, D. Harter, M. A. Arbore, M. Proctor, and M. M. Fejer, Opt. Lett. **23**, 864 (1998).
[134] R. A. Griffin, D. D. Sampson, and D. A. Jackson, J. Lightwave Technol. **13**, 1826 (1995).
[135] H. Soñajalg, A. Débarre, J.-L. Le Gouët, I. Lorgeré, and P. Tchénio, J. Opt. Soc. Am. B **12**, 1448 (1995).
[136] V. Binjrajka, C.-C. Chang, A. W. R. Emanuel, D. E. Leaird, and A. M. Weiner, Opt. Lett. **21**, 1756 (1996).
[137] M. Tian, F. Grelet, I. Lorgere, J.-P. Galaup, and J.-L. Le Gouet, J. Opt. Soc. Am. B **16**, 74 (1999).
[138] M. C. Nuss and R. L. Morrison, Opt. Lett. **20**, 740 (1995).
[139] M. M. Wefers, K. A. Nelson, and A. M. Weiner, Opt. Lett. **21**, 746 (1996).
[140] R. M. Koehl, T. F. Crimmins, C. J. Brennan, and K. A. Nelson, in *Ultrafast Phenomena XI*, edited by T. Elsaesser, J. G. Fujimoto, D. A. Wiersma, and W. Zinth (Springer, Berlin, 1998), pp. 92–94.
[141] K. Hill and D. Brady, Opt. Lett. **18**, 1739 (1993).
[142] K. B. Hill, K. G. Purchase, and D. J. Brady, Opt. Lett. **20**, 1201 (1995).
[143] P. Emplit, J. P. Hamaide, F. Reynaud, C. Froehly, and A. Barthelemy, Opt. Commun. **62**, 374 (1987).
[144] Ph. Emplit, J.-P. Hamaide, and F. Reynaud, Opt. Lett. **17**, 1358 (1992).
[145] D. E. Leaird and A. M. Weiner, Opt. Lett. **24**, 853 (1999).
[146] K. W. Goossen *et al.*, IEEE Photonics Technol. Lett. **7**, 360 (1995).
[147] S. J. B. Yoo, R. Bhat, C. Caneau, J. Gamelin, M. A. Koza, and T. P. Lee, presented at the Optical Fiber Communications Conference, San Diego, CA, 1995.
[148] Y. T. Mazurenko, Appl. Phys. B: Photophys. Laser Chem. **50**, 101 (1990).
[149] A. M. Weiner, D. E. Leaird, D. H. Reitze, and E. G. Paek, Opt. Lett. **17**, 224 (1992).
[150] A. M. Weiner, D. E. Leaird, D. H. Reitze, and E. G. Paek, IEEE J. Quantum Electron. **28**, 2251 (1992).
[151] A. M. Weiner and D. E. Leaird, Opt. Lett. **19**, 123 (1994).
[152] Y. Ding, A. M. Weiner, M. R. Melloch, and D. D. Nolte, Appl. Phys. Lett. **75**, 3255 (1999).
[153] K. Ema and F. Shimizu, Jpn. J. Appl. Phys., Part 1 **29**, 1458 (1990).
[154] P. C. Sun, Y. T. Mazurenko, W. S. C. Chang, P. K. L. Yu, and Y. Fainman, Opt. Lett. **20**, 1728 (1995).
[155] Y. Ding, D. D. Nolte, M. R. Melloch, and A. M. Weiner, Opt. Lett. **17**, 1101 (1997).
[156] D. M. Marom, D. Panasenko, P. C. Sun, and Y. Fainman, Opt. Lett. **24**, 563 (1999).
[157] M. C. Nuss, M. Li, T. H. Chiu, A. M. Weiner, and A. Partovi, Opt. Lett. **19**, 664 (1994).
[158] K. Ema, M. Kuwata-Gonokami, and F. Shimizu, Appl. Phys. Lett. **59**, 2799 (1991).
[159] Y. T. Mazurenko, S. E. Putilin, A. G. Spiro, A. G. Beliaev, V. E. Yashin, and S. A. Chizhov, Opt. Lett. **21**, 1753 (1996).
[160] P. C. Sun, Y. T. Mazurenko, and Y. Fainman, J. Opt. Soc. Am. A **14**, 1159 (1997).
[161] A. M. Kanan and A. M. Weiner, J. Opt. Soc. Am. B **15**, 1242 (1998).
[162] Ph. Emplit, M. Haelterman, and J.-P. Hamaide, Opt. Lett. **18**, 1047 (1993).
[163] W. S. Warren, Science **242**, 878 (1988).
[164] D. Zaccarin and M. Kavehrad, IEEE Photonics Technol. Lett. **5**, 479 (1993).
[165] M. Kavehrad and D. Zaccarin, J. Lightwave Technol. **13**, 534 (1995).
[166] L. Nguyen, T. Dennis, B. Aazhang, and J. F. Young, J. Lightwave Technol. **15**, 1647 (1997).
[167] J. S. Patel and Y. Silberberg, IEEE Photonics Technol. Lett. **7**, 514 (1995).
[168] H. Shi, J. Finlay, G. Alphonse, J. Connolly, and P. J. Delfyett, IEEE Photonics Technol. Lett. **9**, 1439 (1997).
[169] T. Konishi and Y. Ichioka, J. Opt. Soc. Am. A **16**, 1076 (1999).
[170] C. J. Bardeen, V. V. Yakovlev, J. A. Squier, K. R. Wilson, S. Carpenter, and P. Weber, J. Biomed. Opt. **4**, 362 (1999).
[171] W. E. White, F. G. Patterson, R. L. Combs, D. F. Price, and R. L. Shepherd, Opt. Lett. **18**, 1343 (1993).
[172] M. Ulman, D. S. Bailey, L. H. Acioli, F. G. Vallee, C. J. Stanton, E. P. Ippen, and J. G. Fujimoto, Phys. Rev. B **47**, 10267 (1993).
[173] G. D. Sanders, C. K. Sun, J. G. Fujimoto, H. K. Choi, C. A. Wang, and C. J. Stanton, Phys. Rev. B **50**, 8539 (1994).
[174] H. Giessen *et al.*, J. Opt. Soc. Am. B **13**, 1039 (1996).
[175] M. P. Deboer and H. G. Muller, J. Phys. B **27**, 721 (1994).
[176] Z. Zheng, A. M. Weiner, J. H. Marsh, and M. M. Karkhanehchi, IEEE Photonics Technol. Lett. **9**, 493 (1997).
[177] J. J. Baumberg, A. Armitage, M. S. Skolnick, and J. S. Roberts, Phys. Rev. Lett. **81**, 661 (1998).
[178] M. Hase, T. Itano, K. Mizoguchi, and S. Nakashima, Jpn. J. Appl. Phys., Part 2 **37**, L281 (1998).
[179] N. F. Scherer, A. J. Ruggiero, M. Du, and G. R. Fleming, J. Chem. Phys. **93**, 856 (1990).

[180] N. F. Scherer *et al.*, J. Chem. Phys. **95**, 1487 (1991).
[181] B. Kohler *et al.*, J. Phys. Chem. **97**, 12602 (1993).
[182] J. L. Krause, R. M. Whitnell, K. R. Wilson, Y. J. Yan, and S. Mukamel, J. Chem. Phys. **99**, 6562 (1993).
[183] Y. J. Yan, R. E. Gillian, R. M. Whitnell, K. R. Wilson, and S. Mukamel, J. Phys. Chem. **97**, 2320 (1993).
[184] B. Amstrup, R. J. Carlson, A. Matro, and S. A. Rice, J. Phys. Chem. **95**, 8019 (1991).
[185] H. Rabitz, in *Atomic and Molecular Processes with Short Intense Pulses*, edited by A. D. Bandrauk (Plenum, New York, 1988).
[186] S. Shi and H. Rabitz, J. Chem. Phys. **92**, 2927 (1990).
[187] P. Gross, D. Neuhauser, and H. Rabitz, J. Chem. Phys. **96**, 2834 (1992).
[188] D. J. Tannor and S. A. Rice, Adv. Chem. Phys. **70**, 441 (1988).
[189] J. J. Baumberg, in *Semiconductor Quantum Optoelectronics—From Quantum Physics to Smart Devices*, edited by A. Miller and M. Ebrahimzadeh (IOP, Bristol, 1999).
[190] D. Meshulach and Y. Silberberg, Nature (London) **396**, 239 (1998).
[191] B. Broers, L. D. Noordam, and H. B. van Linden van den Heuvell, presented at the International Symposium on Ultrafast Processes in Spectroscopy, Bayreuth, 1991.
[192] B. Broers, L. D. Noordam, and H. B. van Linden van den Heuvall, Phys. Rev. A **46**, 2749 (1992).
[193] Y. Liu, S.-G. Park, and A. M. Weiner, IEEE J. Sel. Top. Quantum Electron. **2**, 709 (1996).
[194] C. W. Siders, J. L. W. Siders, A. J. Taylor, S.-G. Park, M. R. Melloch, and A. M. Weiner, Opt. Lett. **24**, 241 (1999).
[195] D. Umstadter, E. Esarey, and J. Kim, Phys. Rev. Lett. **72**, 1224 (1994).
[196] D. Umstadter, J. Kim, E. Esarey, E. Dodd, and T. Neubert, Phys. Rev. E **51**, 3484 (1995).
[197] D. L. Fisher and T. Tajima, Phys. Rev. E **53**, 1844 (1996).
[198] K. Ohkubo *et al.*, Nucl. Instrum. Methods Phys. Res. A **407**, 57 (1998).
[199] F. V. Hartemann, Phys. Plasmas **5**, 2037 (1998).